
ON THE WIDTH SCALING OF NEURAL OPTIMIZERS UNDER MATRIX OPERATOR NORMS I:

ROW/COLUMN NORMALIZATION AND HYPERPARAMETER TRANSFER^{*}

A PREPRINT

Ruihan Xu

University of Chicago
 ruihanx@uchicago.edu
<https://ruihanxx.github.io/>

Jiajin Li

Sauder School of Business
 University of British Columbia
 jiajin.li@sauder.ubc.ca
<https://gerrili1996.github.io/>

Yiping Lu

Industrial Engineering & Management Science
 Northwestern University
 yiping.lu@northwestern.edu
<https://2prime.github.io/>

March 11, 2026

ABSTRACT

A central question in modern deep learning is how to design optimizers whose behavior remains stable as the network width w increases. We address this question by interpreting several widely used neural-network optimizers, including AdamW and Muon, as instances of steepest descent under matrix operator norms. This perspective links optimizer geometry with the Lipschitz structure of the network forward map, and enables width-independent control of both Lipschitz and smoothness constants. However, steepest-descent rules induced by standard $p \rightarrow q$ operator norms lack layerwise composability and therefore cannot provide width-independent bounds in deep architectures. We overcome this limitation by introducing a family of mean-normalized operator norms, denoted $(p, \text{mean}) \rightarrow (q, \text{mean})$, that admit layerwise composability, yield width-independent smoothness bounds, and give rise to practical optimizers such as *rescaled* AdamW, row normalization, and column normalization. The resulting learning rate width-aware scaling rules recover μP scaling [59] as a special case and provide a principled mechanism for cross-width learning-rate transfer across a broad class of optimizers. We further show that Muon can suffer an $O(\sqrt{w})$ worst-case growth in the smoothness constant, whereas a new family of row-normalized optimizers we propose achieves width-independent smoothness guarantees. Based on the observations, we propose MOGA (Matrix Operator Geometry Aware), a width-aware optimizer based only on row/column-wise normalization that enables stable learning-rate transfer across model widths. Large-scale pre-training on GPT-2 and LLaMA shows that MOGA, especially with row normalization, is competitive with Muon while being notably faster in large-token and low-loss regimes.

Keywords Neural-network optimization · Learning-rate transfer · Gradient normalization · L -smoothness

1 Introduction

Recent neural scaling laws [12, 22, 25, 2] offer a clear narrative: Model performance improves predictably with scale, suggesting that larger architectures should yield better results. Yet putting these laws into practice exposes a fundamental gap: They say little about how optimization hyperparameters should vary with width. In practice, for mainstream

^{*}This technical report describes ongoing research. It will be updated as the work progresses.

optimizers such as AdamW [59, 60, 61] and Muon [18], the optimal learning rate is strongly width dependent: A value tuned for a network with 512 hidden units can diverge or slow markedly when the width increases to 2048. This phenomenon reflects a lack of reliable *hyperparameter transfer* across model scales, where tuning calibrated at the small model fails to generalize to the large one. This sensitivity indicates that standard optimizers do not naturally respect architectural scaling. To realize the gains promised by scaling laws, we therefore seek optimization methods whose tuning is width independent. Naturally, we ask:

Can we design optimization methods whose optimal learning rate transfers reliably as network width increases?

We answer this question in the affirmative by viewing existing neural network optimizers, including SignSGD [7], AdamW [26, 33], GradPower [55], and Muon [8, 24], within a unified framework as instances of steepest descent under matrix operator norms [17, 37]. Specifically, we consider the optimization problem $\min_{\Theta} f(\Theta)$, where Θ denotes the network parameters. At iteration t , classical steepest descent in Euclidean geometry (Frobenius norm in the matrix space) selects the unit-norm direction that yields the largest instantaneous decrease of the first-order model:

$$\mathbf{D}^t = \arg \min_{\|\mathbf{D}\|_F=1} \langle \nabla f(\Theta^t), \mathbf{D} \rangle = - \frac{\nabla f(\Theta^t)}{\|\nabla f(\Theta^t)\|_F}.$$

More generally, steepest descent can be defined with respect to an arbitrary norm $\|\cdot\|$ with dual norm $\|\cdot\|_*$. Different choices of geometry induce different update rules that exploit problem-specific structure. For example, when $\|\cdot\| = \|\cdot\|_p$ with $p \geq 1$, the induced ℓ_{p^*} normalization, where $\frac{1}{p} + \frac{1}{p^*} = 1$, yields the GradPower family of methods [55]. Under ℓ_∞ geometry, the steepest-descent direction reduces to the coordinate-wise sign of the gradient, yielding the well-known SignSGD algorithm [7]. Moreover, AdamW [26, 33] can in fact be viewed as a smoothed or adaptive variant of SignSGD, see Remark 1 for details. Extending steepest-descent geometry from vector spaces to matrix spaces naturally leads to scaling rules governed by matrix operator norms. The resulting descent directions correspond to geometry-aware or “whitened” updates, which can be implemented via row/column normalization or related preconditioning schemes [8, 50, 5, 24, 39, 31]. Viewed from this perspective, the choice of matrix operator norm acts as a versatile design knob that provides a unified geometric framework encompassing a wide range of first-order methods.

Not every operator-norm geometry, however, leads to a practical method. The chosen norm must admit an efficiently computable steepest-descent direction, ideally in closed form or via a fast approximation. Recent work provides simple descent oracles for several families, including Newton–Schulz iteration for $2 \rightarrow 2$ norms, column normalization for $1 \rightarrow q$, and row normalization for $p \rightarrow \infty$. In this paper, we restrict attention to these computationally tractable cases (i.e., $p \rightarrow q$ with $p \leq q$) and investigate whether their induced geometries preserve width-insensitive optimization properties of the network loss.

As an initial step, following the viewpoint of [4, 28], we focus on geometries under which the Lipschitz constant of the loss with respect to weight perturbations does not deteriorate as width increases. To formalize this discussion, we introduce the matrix operator norm induced by vector norms.

Definition 1 (Matrix Operator Norm). *Let $\mathbf{D} \in \mathbb{R}^{m \times n}$, $\|\cdot\|_{\text{in}}$ and $\|\cdot\|_{\text{out}}$ be norms on \mathbb{R}^n and \mathbb{R}^m , respectively. The operator norm of \mathbf{D} induced by these norms is defined as*

$$\|\mathbf{D}\|_{\text{in} \rightarrow \text{out}} := \sup_{\mathbf{x} \in \mathbb{R}^n, \mathbf{x} \neq \mathbf{0}} \frac{\|\mathbf{D}\mathbf{x}\|_{\text{out}}}{\|\mathbf{x}\|_{\text{in}}} = \sup_{\|\mathbf{x}\|_{\text{in}}=1} \|\mathbf{D}\mathbf{x}\|_{\text{out}}.$$

Our analysis reveals that, perhaps counterintuitively, classical operator norms of the form $p \rightarrow q$ with $p \leq q$ do not in general provide width-independent Lipschitz control when stacked across multiple layers of a neural network. To see this, consider the directional derivative of the $(i+2)$ -th layer output with respect to the i -th layer weight matrix \mathbf{W}_i . A standard chain-rule calculation shows that its norm decomposes into three factors: the operator norm of the perturbation $\Delta \mathbf{W}_i$, the operator norm of the next-layer weight matrix \mathbf{W}_{i+1} , and a cross-layer mismatch coefficient $\|\mathbf{I}\|_{i,\text{out} \rightarrow i+1,\text{in}}$, where $\|\mathbf{I}\|_{i,\text{out} \rightarrow i+1,\text{in}}$ denotes the operator norm of the identity map between the output space of layer i and the input space of layer $i+1$, capturing the geometric mismatch between consecutive layers. When this mismatch coefficient exceeds one, even small perturbations can be amplified purely due to geometric inconsistency across consecutive layers. This observation motivates a compatibility condition between adjacent norms, i.e., $\|\cdot\|_{\text{in}} \leq \|\cdot\|_{\text{out}}$. Under this condition, the Lipschitz constant bound remains width independent. However, classical operator norms $p \rightarrow q$ with $1 \leq p < q$ violate this property, i.e., $\|\mathbf{x}\|_p \leq n^{1/p-1/q} \|\mathbf{x}\|_q$, which implies $\|\mathbf{I}\|_{q \rightarrow p} = n^{1/p-1/q} > 1$. These observations motivate introducing a new, width-aware geometry that enforces cross-layer compatibility. To this end, we consider the mean-normalized norms $\|\cdot\|_{(p,\text{mean})}$ defined by

$$\|\mathbf{x}\|_{(p,\text{mean})} := \left(\frac{1}{n} \sum_{i=1}^n |\mathbf{x}_i|^p \right)^{1/p} = n^{-1/p} \|\mathbf{x}\|_p.$$

The factor $n^{-1/p}$ precisely cancels the dimensional scaling of the ℓ_p embeddings, thereby enforcing a compatibility condition between adjacent norms: $\|\mathbf{I}\|_{(q,\text{mean}) \rightarrow (p,\text{mean})} \leq 1$, for all $1 \leq p \leq q \leq \infty$. As a consequence, under the $(p, \text{mean}) \rightarrow (q, \text{mean})$ geometry, the network loss admits a width-independent Lipschitz bound, see Theorem 1.

Beyond width-independent Lipschitz control, a second requirement we consider is whether the operator geometry also admits a width-independent smoothness constant, which governs the curvature of the loss landscape and the stability of gradient-based updates. Theorem 2 shows that the smoothness constant is width independent whenever $q \geq 2p$. More generally, any residual width dependence scales as $w^{\frac{1}{q} - \frac{1}{2p}}$, precisely characterizing how curvature grows with the layer width. In particular, $(1, \text{mean}) \rightarrow (q, \text{mean})$ with $q \geq 2$ and $(p, \text{mean}) \rightarrow \infty$ both yield smoothness bounds that are independent of the network width. By contrast, the $(2, \text{mean}) \rightarrow (2, \text{mean})$ geometry (corresponding to Muon) exhibits a smoothness constant that grows on the order of \sqrt{w} .

Passing from the classical $p \rightarrow q$ geometry to the $(p, \text{mean}) \rightarrow (q, \text{mean})$ geometry induces a principled width-aware rescaling of the learning rate. Indeed, the mean-normalized norm $\|\cdot\|_{(p,\text{mean})}$ differs from the standard ℓ_p norm on \mathbb{R}^n only by a multiplicative factor of $n^{1/p}$. Consequently, the two geometries induce identical update directions up to a dimension-dependent scaling, which can be absorbed into the step size. This observation gives rise to a new family of practical optimizers with explicit width-aware learning-rate rules, referred to as *MOGA* (Matrix Operator Geometry Aware), including rescaled variants of AdamW as well as row and column normalization methods. Moreover, in the special cases of Adam and SignSGD, the resulting scaling coincides exactly with the μP scaling rule of [60]. Importantly, however, the underlying principles behind hyperparameter transfer are conceptually different. μP is motivated by preserving feature-learning behavior as width grows (e.g., keeping feature-level update magnitudes non-degenerate), whose formal theoretical analysis relies on the spectral condition of the network parameterization [61]. In contrast, our scaling arises from an optimization-geometric perspective, through width-independent Lipschitz and smoothness control under mean-normalized operator norms. This viewpoint applies to a broader class of optimizers—including regimes that do not satisfy the spectral assumptions required by μP —while still enabling reliable hyperparameter transfer across widths. Our analysis therefore provides a principled and more general foundation for hyperparameter transfer across model scales.

To summarize, under the mean-normalized operator-norm geometries $(1, \text{mean}) \rightarrow (q, \text{mean})$ with $q \geq 2$ and $(p, \text{mean}) \rightarrow \infty$, the network loss admits width-independent Lipschitz and smoothness bounds with respect to weight perturbations. The induced steepest-descent updates lead to practical optimization methods, in particular a family of rescaled row-normalization algorithms that exhibit reliable learning-rate transfer across widths in our experiments. In contrast, for the recently proposed and widely studied Muon optimizer, which corresponds to the $(2, \text{mean}) \rightarrow (2, \text{mean})$ geometry, our theory reveals a more nuanced picture: Although Muon attains width-independent Lipschitz control, its smoothness constant can grow on the order of \sqrt{w} in the worst case. This reveals a potential limitation of Muon in maintaining stable optimization behavior as width increases, and highlights an advantage of the new rescaled row-normalization family proposed in this paper.

Finally, we validate our theoretical findings through large-scale language model pre-training experiments on both GPT-2 and LLaMA architectures. Consistent with our analysis, the proposed MOGA scaling enables reliable learning-rate transfer across model widths: Models with substantially different parameter counts achieve their best performance at nearly the same peak learning rate, eliminating the need for extensive retuning when scaling up model size. We further evaluate MOGA instantiated with row normalization under both standard and large token budgets, corresponding to approximately $\sim 1\times$ and $\sim 8\times$ the Chinchilla-optimal training tokens [23], respectively, on GPT-2 Small and LLaMA-130M. Across architectures, MOGA instantiated with row normalization achieves competitive or superior optimization performance compared with strong baselines including AdamW and Muon. In particular, under the large-token regime, MOGA instantiated with row normalization demonstrates a clear advantage in the later stages of training and in the low-loss regime, where optimization stability becomes increasingly critical. These results highlight the practical value of width-aware optimizer design: Beyond enabling hyperparameter transfer, the proposed *width-aware rescaled row-normalization optimizer* (i.e., MOGA instantiated with row normalization) can improve training efficiency in regimes that are most relevant for large-scale model deployment.

Notation. Let $\mathbf{x} \in \mathbb{R}^n$ be a column vector, and denote its i -th entry by x_i , $i = 1, \dots, n$. Let $\mathbf{D} \in \mathbb{R}^{m \times n}$ be a matrix. We write $\mathbf{D}_{r,:}$ for the r -th row of \mathbf{D} and $\mathbf{D}_{:,c}$ for its c -th column, for $r = 1, \dots, m$ and $c = 1, \dots, n$. For two vectors $\mathbf{x}, \mathbf{y} \in \mathbb{R}^n$, their elementwise product is defined as $(\mathbf{x} \odot \mathbf{y})_i := x_i y_i$, $i = 1, \dots, n$. Let $f : \Omega \rightarrow \mathbb{R}$ be differentiable, where $\Omega \subset \mathbb{R}^{m \times n}$. For $\mathbf{Z} \in \Omega$ and a direction $\Delta\mathbf{Z}$, the directional derivative of f at \mathbf{Z} along $\Delta\mathbf{Z}$ is defined as

$$\nabla f(\mathbf{Z})[\Delta\mathbf{Z}] := \lim_{t \rightarrow 0} \frac{f(\mathbf{Z} + t\Delta\mathbf{Z}) - f(\mathbf{Z})}{t},$$

whenever the limit exists. Let $f : \Omega \rightarrow \mathbb{R}$ be twice differentiable. For $\mathbf{Z} \in \Omega$ and directions $\Delta\mathbf{Z}_1, \Delta\mathbf{Z}_2$, the directional Hessian of f at \mathbf{Z} is defined as

$$\nabla^2 f(\mathbf{Z})[\Delta\mathbf{Z}_1, \Delta\mathbf{Z}_2] := \lim_{t \rightarrow 0} \frac{\nabla f(\mathbf{Z} + t\Delta\mathbf{Z}_2)[\Delta\mathbf{Z}_1] - \nabla f(\mathbf{Z})[\Delta\mathbf{Z}_1]}{t},$$

whenever the limit exists. We write $a \lesssim b$ if there exists a universal constant $C > 0$, independent of the width, such that $a \leq C b$.

2 Matrix Thinking: Unifying Optimizers via Matrix Operator Norm

We consider the optimization problem of minimizing a neural-network-based loss

$$\min_{\mathbf{W}_{1:\ell}, \mathbf{b}_{1:\ell}} f(\mathbf{W}_{1:\ell}, \mathbf{b}_{1:\ell}) := \mathcal{L}(\mathbf{y}_\ell(\mathbf{x})),$$

where $\mathbf{y}_\ell(\mathbf{x}) \in \mathbb{R}$ denotes the output of a ℓ -layer feedforward neural network with parameters $(\mathbf{W}_{1:\ell}, \mathbf{b}_{1:\ell})$, evaluated at input $\mathbf{x} \in \mathbb{R}^d$. Later on, we write $\Theta := \{\mathbf{W}_{1:\ell}, \mathbf{b}_{1:\ell}\}$ for simplicity.

Definition 2 (Feedforward Neural Network). *Let $\mathbf{y}_0(\mathbf{x}) := \mathbf{x}$. For $i = 1, \dots, K$, define recursively*

$$\mathbf{y}_i(\mathbf{x}) := \sigma(\mathbf{W}_i \mathbf{y}_{i-1}(\mathbf{x}) + \mathbf{b}_i),$$

where $\mathbf{W}_1 \in \mathbb{R}^{w \times d}$, $\mathbf{W}_i \in \mathbb{R}^{w \times w}$ for $i = 2, \dots, K-1$, and $\mathbf{W}_K \in \mathbb{R}^{1 \times w}$. The bias vectors satisfy $\mathbf{b}_i \in \mathbb{R}^w$ for $i = 1, \dots, K-1$ and $b_\ell \in \mathbb{R}$. The hidden states satisfy $\mathbf{y}_i(\mathbf{x}) \in \mathbb{R}^w$ for $i < K$, and the network output is $\mathbf{y}_\ell(\mathbf{x}) \in \mathbb{R}$. Here, σ denotes a activation function, which represents both a mapping $\sigma : \mathbb{R} \rightarrow \mathbb{R}$ and its natural extension $\sigma : \mathbb{R}^n \rightarrow \mathbb{R}^n$, where it is applied pointwise to each component, i.e., $(\sigma(\mathbf{x}))_i = \sigma(x_i)$ for each coordinate i .

Throughout this paper, we assume that the loss function \mathcal{L} and all activation functions σ_i are twice continuously differentiable with uniformly bounded first- and second-order derivatives.

Assumption 1. *Bounded derivatives of activation functions There exist constants $L_\sigma, M_\sigma > 0$ such that*

$$|\sigma'(z)| \leq L_\sigma, \quad \text{and} \quad |\sigma''(z)| \leq M_\sigma, \quad \forall z \in \mathbb{R}.$$

Assumption 2. *Bounded derivatives of the loss function There exist constants $L_J, M_J > 0$ such that*

$$|\mathcal{L}'(z)| \leq L_J, \quad \text{and} \quad |\mathcal{L}''(z)| \leq M_J, \quad \forall z \in \mathbb{R}.$$

With the network architecture and smoothness assumptions in place, we now turn to the central question of this section: how to design and compare first-order optimizers through the geometry they induce. We adopt a matrix operator-norm perspective, viewing many modern optimization methods as instances of steepest-descent updates under appropriately chosen operator norms. This viewpoint encompasses a variety of recent optimizers, including SignSGD [7], Lion [11], and Muon [24], which have demonstrated strong empirical performance in large-scale learning. From this perspective, the choice of geometry plays a dual role. On the one hand, it governs the computational cost of each update through the tractability of the associated steepest-descent direction; on the other hand, it determines the convergence behavior of the resulting optimization method. A well-chosen operator norm must therefore strike a balance between per-iteration computational efficiency and favorable convergence properties.

Computability and per-iteration cost. The steepest-descent direction induced by a general $\|\cdot\|_{p \rightarrow q}$ operator norm does not necessarily admit a closed-form expression. Beyond Muon [24], which employs a Newton–Schulz iteration to approximate steepest descent under the $2 \rightarrow 2$ operator norm, prior work [5] shows that steepest descent under the $1 \rightarrow q$ and $p \rightarrow \infty$ norms admits efficient column-wise and row-wise closed-form computations, respectively. In this paper, we therefore restrict attention to operator norms for which the induced steepest-descent directions are computationally tractable; see Section 2.1 for details.

Convergence speed. Among computable operator norms, a natural question is which (p, q) geometries render the optimization problem well posed and lead to favorable convergence guarantees. We address this question by analyzing the M -Lipschitz continuity (Section 2.2) and L -smoothness (Section 2.3) of neural networks under various $p \rightarrow q$ operator norms.

Our analysis reveals a fundamental limitation of classical *parrow* q operator norms: Both Lipschitz and smoothness constants deteriorate with increasing network width, indicating a structural mismatch between these geometries and the compositional nature of deep neural networks. This degradation arises because standard operator norms fail to propagate stability estimates across layers, thereby distorting the effective geometry of the network’s forward map.

To overcome this issue, we introduce *mean-normalized operator norms*, which are specifically designed to preserve composability under width scaling. These norms yield width-independent first- and second-order estimates and align the optimization geometry with the network’s forward-map geometry. Building on this geometric insight, we develop the MOGA (Matrix Operator Geometry Aware) optimizer and show that μ P-Adam arises as a special case within our framework.

2.1 From AdamW, Muon to Row and Column Normalization

In this subsection, we show that many state-of-the-art optimizers can be interpreted as instances of steepest descent under suitable matrix $p \rightarrow q$ operator norms, with several such instances admitting implementable per-iteration updates [5]. To this end, recall that the steepest-descent direction under a matrix $p \rightarrow q$ operator norm is defined as the solution to

$$\mathbf{D}^* := \arg \min_{\|\mathbf{D}\|_{p \rightarrow q} \leq 1} \langle \nabla f(\Theta), \mathbf{D} \rangle. \quad (1)$$

We begin with three representative optimizers: SignSGD [7], Lion [11], and AdamW [26, 33]. Although these methods were originally developed for optimization over vector-valued parameters, they admit natural interpretations when applied to matrix-valued parameters. At the vector level, both SignSGD and AdamW can be viewed as steepest-descent methods under the ℓ_∞ geometry [3]. When such vector updates are applied entrywise to matrix parameters, the induced geometry corresponds implicitly to the matrix operator norm $\ell_1 \rightarrow \ell_\infty$ [5]. This connection is formalized by the following fact.

Fact 1 ([5], Proposition 3). *Let $\mathbf{D} \in \mathbb{R}^{m \times n}$. Then the element-wise ℓ_∞ norm of \mathbf{D} coincides with its $\ell_1 \rightarrow \ell_\infty$ operator norm, that is,*

$$\|\mathbf{D}\|_{1 \rightarrow \infty} := \sup_{\mathbf{x} \neq 0} \frac{\|\mathbf{D}\mathbf{x}\|_\infty}{\|\mathbf{x}\|_1} = \max_{i,j} |\mathbf{D}_{ij}| =: \|\mathbf{D}\|_{\max}.$$

Then, the steepest-descent subproblem (1) admits the closed-form solution $\mathbf{D}^ = -\text{sign}(\nabla f(\mathbf{W}))$, where $\text{sign}(\cdot)$ is applied entrywise. Consequently, the induced update direction recovers the SignSGD algorithm.*

Remark 1. *We briefly clarify the relationship between Adam, RMSprop, and sign-based methods at the level of update directions. Consider the sign descent update $\theta^{t+1} = \theta^t - \alpha \text{sign}(\tilde{\mathbf{g}}_t)$, where $\tilde{\mathbf{g}}_t$ denotes a (possibly stochastic) gradient estimate and $\alpha > 0$ is the step size. This update corresponds to steepest descent under the ℓ_∞ geometry, as discussed above. The optimizer RMSprop maintains an exponential moving average of squared gradients,*

$$\mathbf{v}^{t+1} = \beta_2 \mathbf{v}^t + (1 - \beta_2) \tilde{\mathbf{g}}^t \odot \tilde{\mathbf{g}}^t, \quad \theta^{t+1} = \theta^t - \alpha \frac{\tilde{\mathbf{g}}^t}{\sqrt{\mathbf{v}^{t+1} + \epsilon}},$$

where $\beta_2 \in [0, 1)$ and $\epsilon > 0$ ensure numerical stability. At the level of update directions, RMSprop (and equivalently Adam with $\beta_1 = 0$) can be viewed as a smoothed variant of sign descent, where the discontinuous sign operator is replaced by a normalized gradient with adaptive, coordinate-wise scaling. Formally, in the limiting case $\beta_2 \rightarrow 0$ and $\epsilon \rightarrow 0$, the RMSprop update reduces to

$$\theta^{t+1} = \theta^t - \alpha \frac{\tilde{\mathbf{g}}^t}{\sqrt{\tilde{\mathbf{g}}^t \odot \tilde{\mathbf{g}}^t}} = \theta^t - \alpha \text{sign}(\tilde{\mathbf{g}}^t),$$

recovering the SignSGD direction. This observation places RMSprop, Adam and AdamW within a broader family of sign-based and geometry-aware first-order methods.

The second example is Muon [24], which can be interpreted as performing steepest descent under the matrix $2 \rightarrow 2$ operator norm. Since the spectral norm of a matrix coincides with the $2 \rightarrow 2$ operator norm, the steepest-descent subproblem (1) admits the closed-form solution $\mathbf{D}^* = -\text{matrixsign}(\nabla f(\Theta))$, where the matrix sign is defined via the singular value decomposition: if $\nabla f(\Theta) = \mathbf{U}\Sigma\mathbf{V}^\top$, then $\text{matrixsign}(\nabla f(\Theta)) = \mathbf{U}\mathbf{V}^\top$. This characterization recovers the update direction of Muon, which whitens or orthogonalizes the gradient matrix. Empirically, Muon has been shown to be an effective alternative to AdamW for large-scale language-model pretraining [31].

The final class of examples consists of the operator norms $\|\cdot\|_{1 \rightarrow q}$ and $\|\cdot\|_{p \rightarrow \infty}$ with $p, q \geq 1$, whose associated steepest-descent subproblems admit closed-form solutions [5, 19]. These geometries induce simple column-wise and row-wise update rules on matrix parameters, see Proposition 1 for details.

Proposition 1. *Consider the steepest-descent subproblem (1) with gradient $\mathbf{G} = \nabla f(\Theta) \in \mathbb{R}^{m \times n}$. For the operator norms $\|\cdot\|_{1 \rightarrow q}$ and $\|\cdot\|_{p \rightarrow \infty}$ with $p, q \geq 1$, the corresponding steepest-descent directions admit the following closed-form expressions:*

(i) *(Column-wise update, $\|\cdot\|_{1 \rightarrow q}$)*

$$\mathbf{D}^* = \text{colnorm}_q(\mathbf{G}) \quad \text{and} \quad \text{colnorm}_q(\mathbf{G})_{:,c} := \frac{\text{sign}(\mathbf{G}_{:,c}) \odot |\mathbf{G}_{:,c}|^{q^*-1}}{\|\mathbf{G}_{:,c}\|_q^{q^*-1}},$$

where $q^ = q/(q-1)$ is the dual exponent.*

(ii) (*Row-wise update*, $\|\cdot\|_{p \rightarrow \infty}$)

$$\mathbf{D}^* = \text{rownorm}_p(\mathbf{G}) \quad \text{and} \quad \text{rownorm}_p(\mathbf{G})_{r,:} := \frac{\text{sign}(\mathbf{G}_{r,:}) \odot |\mathbf{G}_{r,:}|^{p-1}}{\|\mathbf{G}_{r,:}\|_p^{p-1}}.$$

Here \odot denotes elementwise multiplication.

Proof. Proof of Proposition 1. By [5, Proposition 8], the operator norms admit the representations

$$\|\mathbf{D}\|_{1 \rightarrow q} = \max_{c \in [n]} \|\mathbf{D}_{:,c}\|_q, \quad \text{and} \quad \|\mathbf{D}\|_{p \rightarrow \infty} = \max_{r \in [m]} \|\mathbf{D}_{r,:}\|_{p^*},$$

where $p^* = p/(p-1)$ denotes the dual exponent. As a consequence, the steepest-descent subproblem (1) under the $\|\cdot\|_{1 \rightarrow q}$ and $\|\cdot\|_{p \rightarrow \infty}$ operator norms decouples across columns and rows, respectively.

We focus on the case $\|\cdot\|_{1 \rightarrow q}$ for illustration; the proof for $\|\cdot\|_{p \rightarrow \infty}$ follows by an analogous argument and is therefore omitted. For the $\|\cdot\|_{1 \rightarrow q}$ case, the steepest-descent subproblem (1) can be written as

$$\min_{\mathbf{D} \in \mathbb{R}^{m \times n}} \langle \mathbf{G}, \mathbf{D} \rangle \quad \text{s.t.} \quad \|\mathbf{D}_{:,c}\|_q \leq 1, \quad \forall c \in [n].$$

Since the objective decomposes as $\langle \mathbf{G}, \mathbf{D} \rangle = \sum_{c=1}^n \langle \mathbf{G}_{:,c}, \mathbf{D}_{:,c} \rangle$, the problem decouples across columns. For each column $c \in [n]$, we obtain the subproblem $\min_{\|\mathbf{d}\|_q \leq 1} \langle \mathbf{G}_{:,c}, \mathbf{d} \rangle$. By Hölder's inequality, an optimal solution is given by

$$\mathbf{d}^* = - \frac{\text{sign}(\mathbf{G}_{:,c}) \odot |\mathbf{G}_{:,c}|^{q^*-1}}{\|\mathbf{G}_{:,c}\|_{q^*}^{q^*-1}},$$

where $q^* = q/(q-1)$ is the dual exponent. Collecting the solutions for all columns yields $\mathbf{D}^* = \text{colnorm}_q(\mathbf{G})$, which completes the proof. \square

Message: Although SignSGD/AdamW is typically formulated under the vector ℓ_∞ norm, it can also be interpreted through the lens of a matrix $\ell_1 \rightarrow \ell_\infty$ norm. In a similar vein, Muon [24, 8] performs steepest descent under the $\ell_2 \rightarrow \ell_2$ operator norm. More generally, our framework considers the full families of operator norms $\ell_1 \rightarrow \ell_q$ and $\ell_p \rightarrow \ell_\infty$ for arbitrary $p, q \geq 1$, which induce column-wise and row-wise normalization updates, respectively. Several existing methods studied in the literature can be recovered as special cases corresponding to particular choices of (p, q) ; for instance, [19, 46] focus on the $\ell_1 \rightarrow \ell_2$ case, while [5, 34] consider the $\ell_2 \rightarrow \ell_\infty$ geometry. This perspective highlights the underlying **matrix thinking** behind a broad class of first-order optimizers. Notably, the update rules induced by the $\ell_1 \rightarrow \ell_q$ and $\ell_p \rightarrow \ell_\infty$ families admit efficient, vectorized implementations.

SignSGD/AdamW	Column Normalization	Row Normalization	Muon
$\ \cdot\ _{1 \rightarrow \infty}$	$\ \cdot\ _{1 \rightarrow q}$	$\ \cdot\ _{p \rightarrow \infty}$	$\ \cdot\ _{2 \rightarrow 2}$

In summary, all matrix $p \rightarrow q$ operator norms that admit implementable per-iteration updates fall within the regime $p \leq q$. Accordingly, we focus on the case $p \rightarrow q$ with $p \leq q$ in the remainder of the paper.

2.2 Width-independent Lipschitz Bound under Mean-Normalized Geometry

Section 2.1 shows that a broad class of first-order optimizers can be interpreted as steepest-descent methods under matrix $p \rightarrow q$ operator norms ($p \leq q$) with computable update rules. A natural next question is whether these classical operator-norm geometries are well aligned with the stability properties of deep neural networks. In particular, the chosen matrix norm should reflect the model's sensitivity to weight perturbations so that the loss remains width-independent Lipschitz continuous [6, 4, 28]. However, despite their computational tractability and clean geometric form, we show that classical $p \rightarrow q$ operator norms with $p \leq q$ generally fail to yield width-independent Lipschitz bounds for neural networks. As a result, the induced Lipschitz bounds deteriorate with network width under these norms. This structural limitation motivates a refined geometry. In the remainder of this subsection, we introduce mean-normalized operator norms and show that they do yield width-independent Lipschitz bounds, see Theorem 1 for details.

To quantify the Lipschitz behavior induced by a given operator norm, we start to analyze the network in a layer-wise manner and track how Lipschitz bounds compose across layers. We model the network as a composition of linear maps and nonlinear activation functions:

$$\mathbf{y}_{\ell+1} = \sigma(\mathbf{z}_{\ell+1}), \quad \text{and} \quad \mathbf{z}_{\ell+1} = \mathbf{W}_{\ell+1} \mathbf{y}_\ell + \mathbf{b}_{\ell+1},$$

where $\mathbf{z}_{\ell+1}$ denotes the pre-activation.

Each linear layer \mathbf{W}_ℓ maps features from one normed space to the next pre-activation space. When \mathbf{W}_ℓ is endowed with the operator norm $\|\cdot\|_{\text{in}\rightarrow\text{out}}$, Lipschitz stability propagates layer by layer. In particular, if σ is 1-Lipschitz, then the sensitivity of $\mathbf{y}_{\ell+1}$ to perturbations in an earlier weight matrix \mathbf{W}_i ($i < \ell + 1$) satisfies

$$\|\nabla_{\mathbf{W}_i} \mathbf{y}_{\ell+1}\|_{\text{out}} \leq \|\nabla_{\mathbf{W}_i} \mathbf{z}_{\ell+1}\|_{\text{out}} = \|\mathbf{W}_{\ell+1} \nabla_{\mathbf{W}_i} \mathbf{y}_\ell\|_{\text{out}} \leq \|\mathbf{W}_{\ell+1}\|_{\text{in}\rightarrow\text{out}} \|\nabla_{\mathbf{W}_i} \mathbf{y}_\ell\|_{\text{in}},$$

where $\nabla_{\mathbf{W}_i} \mathbf{y}_\ell$ denotes the Jacobian of \mathbf{y}_ℓ with respect to \mathbf{W}_i . Similarly, by the definition of the induced operator norm of $\mathbf{W}_{\ell+2}$, we have $\|\nabla_{\mathbf{W}_i} \mathbf{y}_{\ell+2}\|_{\text{out}} \leq \|\mathbf{W}_{\ell+2}\|_{\text{in}\rightarrow\text{out}} \|\nabla_{\mathbf{W}_i} \mathbf{y}_{\ell+1}\|_{\text{out}}$. To compose this bound with the previous layer-wise estimate, the output norm of layer $\ell + 1$ must be compatible with the input norm of layer $\ell + 2$. That is, we impose the following norm-compatibility condition between consecutive layers:

$$\|\cdot\|_{\text{in}} \leq \|\cdot\|_{\text{out}}. \quad (2)$$

Under the compatibility condition (2), the layer-wise bounds compose and yield

$$\|\nabla_{\mathbf{W}_i} \mathbf{y}_{\ell+2}\|_{\text{in}} \leq \|\mathbf{W}_{\ell+2}\|_{\text{in}\rightarrow\text{out}} \|\nabla_{\mathbf{W}_i} \mathbf{y}_{\ell+1}\|_{\text{out}} \leq \left(\prod_{k=i+1}^{\ell+2} \|\mathbf{W}_k\|_{\text{in}\rightarrow\text{out}} \right) \|\nabla_{\mathbf{W}_i} \mathbf{y}_i\|_{\text{in}}.$$

From the layer-wise bounds derived above, a width-independent cross-layer stability estimate based on operator norms is valid only if the input and output norms across consecutive layers satisfy the compatibility condition (2). This ensures that the sensitivity bounds can be composed across layers without distortion and therefore imposes a structural constraint on the admissible operator-norm geometries. However, classical matrix-induced norm families—such as the $1 \rightarrow q$ and $p \rightarrow \infty$ cases that admit closed-form steepest-descent directions—do not meet this compatibility requirement in a dimension-independent manner. The difficulty is that the underlying feature norms are not uniformly comparable across layers. Indeed, ℓ_p norms are not uniformly equivalent: for $\mathbf{x} = (1, \dots, 1) \in \mathbb{R}^n$ and any $p > 1$, $\|\mathbf{x}\|_\infty = 1 < \|\mathbf{x}\|_p = n^{1/p} < \|\mathbf{x}\|_1 = n$, so the norm ratios grow with dimension.

To remove this dimension dependence, we introduce a mean-normalized variant of the p -power norm and work with the $(p, \text{mean}) \rightarrow (q, \text{mean})$ operator-norm geometry instead of the standard $p \rightarrow q$ setting. Formally, for $\mathbf{x} \in \mathbb{R}^n$ and $1 \leq p < \infty$, we define the (p, mean) norm by

$$\|\mathbf{x}\|_{(p, \text{mean})} := \left(\frac{1}{n} \sum_{i=1}^n |x_i|^p \right)^{1/p}. \quad (3)$$

This family recovers several familiar quantities as special cases: $\|\cdot\|_{(1, \text{mean})}$ equals the mean absolute value (MAV), $\|\cdot\|_{(2, \text{mean})}$ equals the root mean square (RMS), and $\|\cdot\|_{(\infty, \text{mean})}$ reduces to the maximum norm, i.e., $\|\mathbf{x}\|_\infty = \max_i |x_i|$. This normalization rescales the classical ℓ_p norm by the width factor and removes dimension-dependent growth. The key property of the (p, mean) norms is that they remain uniformly comparable across widths.

Fact 2 (Monotonicity of (p, mean) norms). *Let $\mathbf{x} \in \mathbb{R}^n$ and $1 \leq p < q \leq \infty$. Then*

$$\|\mathbf{x}\|_{(p, \text{mean})} \leq \|\mathbf{x}\|_{(q, \text{mean})}.$$

Proof. Proof of Fact 2. The claim follows from the generalized mean inequality: For any $a_i \geq 0$ and $1 \leq p \leq q$,

$$\left(\frac{1}{n} \sum_{i=1}^n a_i^p \right)^{1/p} \leq \left(\frac{1}{n} \sum_{i=1}^n a_i^q \right)^{1/q}.$$

Apply this inequality with $a_i = |x_i|$ yields the result. □

We now establish a width-independent Lipschitz bound for neural networks under the general $(p, \text{mean}) \rightarrow (q, \text{mean})$ operator-norm geometry.

Theorem 1 (Width-independent Lipschitz bound under mean-normalized geometry). *Consider a K -layer neural network defined in Definition 2 with activation function σ and loss \mathcal{L} satisfying Assumptions 1–2. Let $1 \leq p \leq q < \infty$, and suppose the input satisfies $\|\mathbf{x}\|_2 \leq C$ for some $C > 1$. Define the parameter set as $\Omega_C := \{\Theta : \|\Theta\|_{\text{block}} \leq C\}$, where the block norm $\|\Theta\|_{\text{block}}$ is defined as*

$$\max \left\{ \|\mathbf{W}_1\|_{1 \rightarrow (q, \text{mean})}, \max_{2 \leq i \leq K-1} \|\mathbf{W}_i\|_{(p, \text{mean}) \rightarrow (q, \text{mean})}, \|\mathbf{W}_K\|_{(p, \text{mean}) \rightarrow \infty}, \max_i \|\mathbf{b}_i\|_\infty \right\}. \quad (4)$$

Then the loss function is Lipschitz continuous on Ω_C , i.e.,

$$|f(\Theta) - f(\Theta')| \leq M_{\text{net}} \|\Theta - \Theta'\|_{\text{block}} \quad \forall \Theta, \Theta' \in \Omega_C,$$

where $M_{\text{net}} > 0$ depends only on C, K , and the constants in Assumptions 1–2, and is independent of all layer widths.

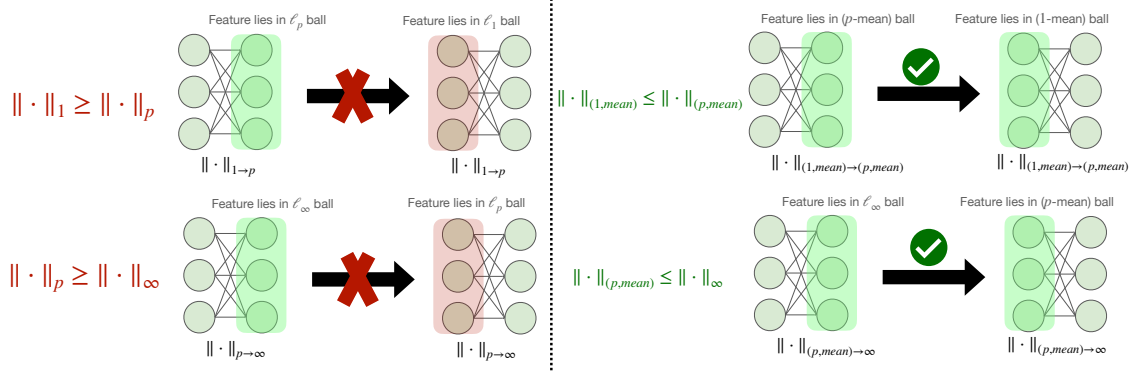


Figure 1: **Operators Should Play Nice Together.** Chaining layer-wise stability bounds under $\|\cdot\|_{p \rightarrow q}$ requires $\|\cdot\|_p \leq \|\cdot\|_q$. This fails for classical $p \rightarrow q$ norms when $p \leq q$ but holds for $(p, \text{mean}) \rightarrow (q, \text{mean})$ norms, yielding dimension-independent bounds.

Remark 2 (Why the bounded parameter set is natural). *The restriction $\Theta \in \Omega_C$ is natural in practice, as standard training procedures implicitly control parameter norms. Under the standard decoupled weight-decay update, $\Theta^{t+1} = (1 - \eta\lambda)\Theta^t + \eta\mathbf{D}^t$, where $\eta > 0$, $0 < \lambda < 1$ and $\|\mathbf{D}^t\| \leq 1$, we have $\|\Theta^{t+1}\| \leq (1 - \eta\lambda)\|\Theta^t\| + \eta$. Unrolling the recursion gives $\|\Theta^t\| \leq (1 - \eta\lambda)^t\|\Theta^0\| + 1/\lambda$, and hence $\sup_t \|\Theta^t\| \leq O(1/\lambda)$. Thus, weight decay together with bounded update directions keeps the parameters in a uniformly bounded ball. Moreover, several modern optimizers admit equivalent formulations as optimization under explicit norm constraints [10, 9, 39], further supporting the bounded-parameter assumption.*

We now turn to the proof of Theorem 1.

Proof. Proof of Theorem 1. We prove the Lipschitz continuity of $f(\Theta) = \mathcal{L}(y_K(\Theta); x)$ on Ω_C with respect to $\|\cdot\|_{\text{block}}$ by invoking Lemma 1. It suffices to show the following *uniform directional-derivative bound*:

$$\sup_{\|\Delta\Theta\|_{\text{block}} \leq 1} |\nabla f(\Theta)[\Delta\Theta]| \leq M_{\text{net}}, \quad \forall \Theta \in \Omega_C, \quad (5)$$

for some constant M_{net} that does not depend on the width w . By the chain rule and Assumption 2, we have $|\nabla f(\Theta)[\Delta\Theta]| \leq L_J |\nabla y_K(\Theta)[\Delta\Theta]|$. Therefore, to prove (5), it is enough to bound $|\nabla y_K(\Theta)[\Delta\Theta]|$ uniformly over $\Theta \in \Omega_C$ and $\|\Delta\Theta\|_{\text{block}} \leq 1$. We decompose

$$\nabla y_K(\Theta)[\Delta\Theta] = \sum_{j=1}^K \nabla_{\mathbf{W}_j} y_K(\Theta)[\Delta\mathbf{W}_j] + \sum_{j=1}^K \nabla_{\mathbf{b}_j} y_K(\Theta)[\Delta\mathbf{b}_j].$$

Then, it suffices to establish width-independent bounds on each term $\nabla_{\mathbf{W}_j} y_K[\Delta\mathbf{W}_j]$ and $\nabla_{\mathbf{b}_j} y_K[\Delta\mathbf{b}_j]$.

We first establish a uniform bound on the intermediate hidden states $y_i(\Theta)$ for $i = 1, \dots, K-1$. Since $\sigma(0) = 0$ and $|\sigma'(z)| \leq L_\sigma$, the mean-value theorem implies $|\sigma(z)| \leq L_\sigma |z|$ for all $z \in \mathbb{R}$. Applying this componentwise yields

$$\|\sigma(\mathbf{x})\|_{(q, \text{mean})} \leq L_\sigma \|\mathbf{x}\|_{(q, \text{mean})}, \quad \forall \mathbf{x} \in \mathbb{R}^d \text{ and } q \geq 1. \quad (6)$$

Fix any $\Theta \in \Omega_C$ and $\|\mathbf{x}\|_2 \leq C$. Using (6) and the definition of $\|\Theta\|_{\text{block}} \leq C$, we have

$$\|\mathbf{y}_1\|_{(q, \text{mean})} = \|\sigma(\mathbf{W}_1 \mathbf{x} + \mathbf{b}_1)\|_{(q, \text{mean})} \leq L_\sigma \left(\|\mathbf{W}_1\|_{1 \rightarrow (q, \text{mean})} \|\mathbf{x}\|_1 + \|\mathbf{b}_1\|_\infty \right) \leq 2L_\sigma C^2.$$

For $2 \leq i \leq K-1$, thanks to Fact 2 and $\|\Theta\|_{\text{block}} \leq C$, we obtain

$$\begin{aligned} \|\mathbf{y}_i\|_{(q, \text{mean})} &= \|\sigma(\mathbf{W}_i \mathbf{y}_{i-1} + \mathbf{b}_i)\|_{(q, \text{mean})} \leq L_\sigma \left(\|\mathbf{W}_i\|_{(p, \text{mean}) \rightarrow (q, \text{mean})} \|\mathbf{y}_{i-1}\|_{(p, \text{mean})} + \|\mathbf{b}_i\|_\infty \right) \\ &\leq L_\sigma (C \|\mathbf{y}_{i-1}\|_{(q, \text{mean})} + C) \leq 2L_\sigma C \max\{1, \|\mathbf{y}_{i-1}\|_{(q, \text{mean})}\} \leq (2L_\sigma C)^i C, \end{aligned} \quad (7)$$

which is independent of the width w .

We now bound the directional derivative of y_K with respect to each parameter block. Fix any direction $\Delta\Theta = (\Delta\mathbf{W}_{1:K}, \Delta\mathbf{b}_{1:K})$ with $\|\Delta\Theta\|_{\text{block}} \leq 1$. For each $i = 1, \dots, K$, let $\Sigma_i := \text{diag}(\sigma'(z_i))$, so that $\|\Sigma_i\|_\infty \leq L_\sigma$, $i = 1, \dots, K$. For $1 \leq j \leq i \leq K$, we define

$$\Lambda_{i,j}^{\mathbf{W}} := \nabla_{\mathbf{W}_j} y_i[\Delta\mathbf{W}_j] \quad \text{and} \quad \Lambda_{i,j}^{\mathbf{b}} := \nabla_{\mathbf{b}_j} y_i[\Delta\mathbf{b}_j].$$

By the chain rule (essentially the backpropagation rule), for each $i = 1, \dots, K$ and $j = 1, \dots, i$, we have

$$\Lambda_{i,j}^{\mathbf{W}} = \begin{cases} \Sigma_i(\Delta \mathbf{W}_j \mathbf{y}_{i-1}), j = i \\ \Sigma_i \mathbf{W}_i \Lambda_{i-1,j}^{\mathbf{W}}, j < i \end{cases} \text{ and } \Lambda_{i,j}^{\mathbf{b}} = \begin{cases} \Sigma_i \Delta \mathbf{b}_j, j = i \\ \Sigma_i \mathbf{W}_i \Lambda_{i-1,j}^{\mathbf{b}}, j < i \end{cases}. \quad (8)$$

We now bound these quantities case by case.

Case 1: $j = i$. For $2 \leq i \leq K - 1$, using Fact 2, and the bound (7), we obtain

$$\begin{aligned} \|\Lambda_{i,i}^{\mathbf{W}}\|_{(p,\text{mean})} &\leq \|\Lambda_{i,i}^{\mathbf{W}}\|_{(q,\text{mean})} = \|\Sigma_i(\Delta \mathbf{W}_i \mathbf{y}_{i-1})\|_{(q,\text{mean})} \\ &\leq \|\Sigma_i\|_{\infty \rightarrow \infty} \|\Delta \mathbf{W}_i \mathbf{y}_{i-1}\|_{(q,\text{mean})} \leq L_\sigma \|\Delta \mathbf{W}_i\|_{(p,\text{mean}) \rightarrow (q,\text{mean})} \|\mathbf{y}_{i-1}\|_{(p,\text{mean})} \\ &\leq L_\sigma \|\mathbf{y}_{i-1}\|_{(q,\text{mean})} \leq L_\sigma (2L_\sigma C)^{i-1} C, \text{ and} \\ \|\Lambda_{i,i}^{\mathbf{b}}\|_{(p,\text{mean})} &\leq \|\Lambda_{i,i}^{\mathbf{b}}\|_{\infty} = \|\Sigma_i \Delta \mathbf{b}_i\|_{\infty} \leq \|\Sigma_i\|_{\infty} \|\Delta \mathbf{b}_i\|_{\infty} \leq L_\sigma. \end{aligned}$$

For $i = 1$, we have $\Lambda_{1,1}^{\mathbf{W}} = \Sigma_1(\Delta \mathbf{W}_1 \mathbf{x})$ and thus

$$\|\Lambda_{1,1}^{\mathbf{W}}\|_{(q,\text{mean})} \leq L_\sigma \|\Delta \mathbf{W}_1\|_{1 \rightarrow (q,\text{mean})} \|\mathbf{x}\|_1 \leq L_\sigma C,$$

where the last inequality uses $\|\Delta \mathbf{W}_1\|_{1 \rightarrow (q,\text{mean})} \leq 1$ and $\|\mathbf{x}\|_1 \lesssim C$. For the last layer $i = K$, since $\mathbf{y}_K \in \mathbb{R}$, we have

$$\begin{aligned} |\Lambda_{K,K}^{\mathbf{W}}| &= |\Sigma_K(\Delta \mathbf{W}_K \mathbf{y}_{K-1})| \leq L_\sigma \|\Delta \mathbf{W}_K\|_{(p,\text{mean}) \rightarrow \infty} \|\mathbf{y}_{K-1}\|_{(p,\text{mean})} \\ &\leq L_\sigma \|\mathbf{y}_{K-1}\|_{(q,\text{mean})} \leq 2^{K-1} L_\sigma^K C^K. \end{aligned}$$

Finally, $|\Lambda_{1,1}^{\mathbf{b}}| \leq L_\sigma$ and $|\Lambda_{K,K}^{\mathbf{b}}| \leq L_\sigma$ follow similarly.

Case 2: $j < i$ and $i \neq K$. For $j < i \leq K - 1$, we have

$$\begin{aligned} \|\Lambda_{i,j}^{\mathbf{W}}\|_{(p,\text{mean})} &\leq \|\Lambda_{i,j}^{\mathbf{W}}\|_{(q,\text{mean})} = \|\Sigma_i \mathbf{W}_i \Lambda_{i-1,j}^{\mathbf{W}}\|_{(q,\text{mean})} \leq \|\Sigma_i\|_{\infty \rightarrow \infty} \|\mathbf{W}_i \Lambda_{i-1,j}^{\mathbf{W}}\|_{(q,\text{mean})} \\ &\leq L_\sigma \|\mathbf{W}_i\|_{(p,\text{mean}) \rightarrow (q,\text{mean})} \|\Lambda_{i-1,j}^{\mathbf{W}}\|_{(p,\text{mean})} \leq L_\sigma C \|\Lambda_{i-1,j}^{\mathbf{W}}\|_{(p,\text{mean})} \end{aligned} \quad (9)$$

$$\leq (L_\sigma C)^{i-j} \|\Lambda_{j,j}^{\mathbf{W}}\|_{(p,\text{mean})}. \quad (10)$$

Combining with the result of Case 1 yields a width-independent bound on $\|\Lambda_{i,j}^{\mathbf{W}}\|$. Similarly, we have

$$\|\Lambda_{i,j}^{\mathbf{b}}\|_{(p,\text{mean})} \leq (L_\sigma C)^{i-j} \|\Lambda_{j,j}^{\mathbf{b}}\|_{(p,\text{mean})} \leq (L_\sigma C)^{i-j} L_\sigma, \quad (11)$$

which is also width-independent.

Case 3: $j < i = K$. In this case $\mathbf{y}_K \in \mathbb{R}$. We have

$$\begin{aligned} |\Lambda_{K,j}^{\mathbf{W}}| &= |\Sigma_K \mathbf{W}_K \Lambda_{K-1,j}^{\mathbf{W}}| \leq L_\sigma \|\mathbf{W}_K \Lambda_{K-1,j}^{\mathbf{W}}\|_{\infty} \leq L_\sigma \|\mathbf{W}_K\|_{(p,\text{mean}) \rightarrow \infty} \|\Lambda_{K-1,j}^{\mathbf{W}}\|_{(p,\text{mean})} \\ &\leq L_\sigma C \|\Lambda_{K-1,j}^{\mathbf{W}}\|_{(p,\text{mean})}, \text{ and} \\ |\Lambda_{K,j}^{\mathbf{b}}| &\leq L_\sigma C \|\Lambda_{K-1,j}^{\mathbf{b}}\|_{(p,\text{mean})}. \end{aligned}$$

Combining the results from Case 1 and 2 yields the width independent bounds.

By Cases 1–3, there exists a constant $C_\star = C_\star(K, L_\sigma, C)$ independent of the width w such that for all $\Theta \in \Omega_C$ and all directions $\|\Delta \Theta\|_{\text{block}} \leq 1$,

$$|\nabla_{\mathbf{W}_j \mathbf{y}_K}(\Theta)[\Delta \mathbf{W}_j]| \leq C_\star, \quad \text{and} \quad |\nabla_{\mathbf{b}_j \mathbf{y}_K}(\Theta)[\Delta \mathbf{b}_j]| \leq C_\star, \quad j = 1, \dots, K.$$

We conclude our proof. \square

2.3 Width-independent Smoothness Bound under Mean-Normalized Geometry

While [4, 28] suggest choosing norms that reflect the output’s sensitivity to input and weight perturbations, Lipschitz continuity alone provides limited structural information and may not adequately capture the dynamics of deep learning optimization. In this subsection, we further consider how the gradient itself varies along the optimization trajectory, which characterizes the local oscillation of the landscape. This property is known as L -smoothness, or gradient Lipschitz continuity, in optimization. Specifically, it requires that the gradient changes in a controlled manner, meaning that it does not vary too rapidly between nearby points. This property plays a central role in optimization, as it ensures that gradient-based methods can take stable and predictable steps and allows us to bound the decrease in the objective value at each iteration.

To formalize this notion, we introduce the standard concept of L -smoothness.

Definition 3 (L -Smoothness). *Let $f : \Omega \rightarrow \mathbb{R}$ be differentiable on a convex set Ω equipped with a norm $\|\cdot\|$. We say that f is L -smooth with respect to $\|\cdot\|$ if, for all $\mathbf{Z}, \mathbf{Z}' \in \Omega$,*

$$\|\nabla f(\mathbf{Z}) - \nabla f(\mathbf{Z}')\|_* \leq L \|\mathbf{Z} - \mathbf{Z}'\|,$$

where $\|\cdot\|_*$ denotes the dual norm of $\|\cdot\|$.

Recent works [29, 39, 48, 19, 45, 27] have shown that, under an L -smoothness assumption, convergence guarantees of first-order methods can be dimension independent, depending only on the smoothness constant L . This connection can be understood through the standard descent analysis under a general norm geometry. In particular, the steepest descent direction under $\|\cdot\|$ is defined by

$$\mathbf{D}^t = \arg \min_{\|\mathbf{D}\| \leq 1} \langle \nabla f(\mathbf{Z}^t), \mathbf{D} \rangle = -\frac{\nabla f(\mathbf{Z}^t)}{\|\nabla f(\mathbf{Z}^t)\|_*},$$

and the update rule becomes $\mathbf{Z}^{t+1} = \mathbf{Z}^t - \eta^t \mathbf{D}^t$. Since $\langle \nabla f(\mathbf{Z}^t), \mathbf{D}^t \rangle = -\|\nabla f(\mathbf{Z}^t)\|_*$, the L -smoothness condition implies $f(\mathbf{Z}^{t+1}) \leq f(\mathbf{Z}^t) - \eta^t \|\nabla f(\mathbf{Z}^t)\|_* + \frac{1}{2} \eta^t{}^2$. Choosing the optimal step size $\eta^t = \frac{\|\nabla f(\mathbf{Z}^t)\|_*}{L}$ yields

$$f(\mathbf{Z}^{t+1}) \leq f(\mathbf{Z}^t) - \frac{1}{2L} \|\nabla f(\mathbf{Z}^t)\|_*^2.$$

This analysis shows that the optimal learning rate is governed by the smoothness constant L . Therefore, obtaining a width-independent bound on L is crucial for deriving learning-rate rules that remain stable as model width grows, which motivates our study of width-independent smoothness bounds.

Motivated by the above discussion, we next establish width-independent bounds on the smoothness constant under the mean-normalized geometries $(p, \text{mean}) \rightarrow (q, \text{mean})$ considered in this work. Our main result is stated as follows.

Theorem 2. *Consider a K -layer neural network defined in Definition 2 with activation function σ and loss \mathcal{L} satisfying Assumptions 1–2. Let $1 \leq p \leq q \leq \infty$, and suppose the input satisfies $\|\mathbf{x}\|_2 \leq C$ for some $C > 1$. Define the parameter set as $\Omega_C := \{\Theta : \|\Theta\|_{\text{block}} \leq C\}$, where $\|\Theta\|_{\text{block}}$ is defined in (4). Then, we have*

$$\|\nabla f(\Theta) - \nabla f(\Theta')\|_{\text{block}, \star} \leq L_{\text{net}} w^{\max(0, \frac{2}{q} - \frac{1}{p})} \|\Theta - \Theta'\|_{\text{block}} \quad \forall \Theta, \Theta' \in \Omega_C,$$

where $L_{\text{net}} > 0$ depends only on C, K , and the constants in Assumptions 1–2, and is independent of all layer widths.

Remark 3. *As shown in Theorem 2, the smoothness constant exhibits a width dependence of order $w^{\max\{0, 2/q-1/p\}}$ under the $(p, \text{mean}) \rightarrow (q, \text{mean})$ geometry. In particular, the smoothness becomes width independent whenever $q \geq 2p$. Therefore, achieving width-independent smoothness naturally motivates considering geometries with sufficiently large output norms. In addition, for practical optimization algorithms, the steepest descent direction should admit a closed-form expression. Combining these two considerations, our analysis focuses on the $(1, \text{mean}) \rightarrow q$ geometries with $q \geq 2$ and the $(p, \text{mean}) \rightarrow \infty$ geometries.*

Before presenting the proof of Theorem 2, we now explain how the width-dependent factor $w^{\max\{0, 2/q-1/p\}}$ arises in the smoothness bound under the $(p, \text{mean}) \rightarrow (q, \text{mean})$ geometry. Recall that L -smoothness is defined with respect to perturbations in the parameter space. By Lemma 2, it suffices to bound the directional Hessian $\nabla^2 f(\Theta)[\Delta\Theta^1, \Delta\Theta^2]$ uniformly over unit perturbations $\|\Delta\Theta^1\|_{\text{block}}, \|\Delta\Theta^2\|_{\text{block}} \leq 1$. To see the key mechanism, consider a single layer map $\sigma(\mathbf{W}\mathbf{x})$ with a perturbation $\mathbf{W} \mapsto \mathbf{W} + \Delta\mathbf{W}$. Since $\mathbf{W}\mathbf{x}$ is linear in \mathbf{W} , the only nontrivial second-order term comes from the feature-wise nonlinearity σ . In particular, the second-order variation contains the quadratic activation perturbation $(\Delta\mathbf{W}\mathbf{x}) \odot (\Delta\mathbf{W}\mathbf{x})$. Using boundedness of σ'' and the loss derivatives (Assumptions 1–2), the directional Hessian can be reduced to controlling this quadratic term:

$$\left| \nabla^2 f(\mathbf{W})[\Delta\mathbf{W}^1, \Delta\mathbf{W}^2] \right| \lesssim \left\| (\Delta\mathbf{W}^1 \mathbf{x}) \odot (\Delta\mathbf{W}^2 \mathbf{x}) \right\|_{(p, \text{mean})}.$$

Under the $(p, \text{mean}) \rightarrow (q, \text{mean})$ operator-norm geometry, $\|\Delta \mathbf{W}^i \mathbf{x}\|_{(q, \text{mean})}$ is directly controlled by $\|\Delta \mathbf{W}^i\|_{(p, \text{mean}) \rightarrow (q, \text{mean})} \leq 1$. To bound the quadratic term in the (p, mean) norm, we invoke Lemma 4, which yields

$$\|(\Delta \mathbf{W}^1 \mathbf{x}) \odot (\Delta \mathbf{W}^2 \mathbf{x})\|_{(p, \text{mean})} \lesssim w^{\max(0, \frac{2}{q} - \frac{1}{p})} \|\Delta \mathbf{W}^1 \mathbf{x}\|_{(q, \text{mean})} \|\Delta \mathbf{W}^2 \mathbf{x}\|_{(q, \text{mean})}.$$

Combining this with the operator-norm bound $\|\Delta \mathbf{W}^i \mathbf{x}\|_{(q, \text{mean})} \leq \|\Delta \mathbf{W}^i\|_{(p, \text{mean}) \rightarrow (q, \text{mean})} \|\mathbf{x}\|_{(p, \text{mean})}$ shows that the directional Hessian—and hence the smoothness constant—scales as $w^{\max(0, 2/q - 1/p)}$.

With the above preparation, we are now ready to present the proof of Theorem 2. *Proof.* Proof of Theorem 2. We prove the L -smoothness of $f(\Theta) = \mathcal{L}(y_K(\Theta; \mathbf{x}))$ on Ω_C with respect to $\|\cdot\|_{\text{block}}$ by invoking Lemma 2. It suffices to establish the following uniform directional-Hessian bound:

$$\sup_{\|\Delta \Theta^1\|_{\text{block}} \leq 1, \|\Delta \Theta^2\|_{\text{block}} \leq 1} |\nabla^2 f(\Theta)[\Delta \Theta^1, \Delta \Theta^2]| \leq L_{\text{net}}, \quad \forall \Theta \in \Omega_C, \quad (12)$$

for some constant L_{net} . By the chain rule and Assumptions 1–2, we have

$$|\nabla^2 f(\Theta)[\Delta \Theta^1, \Delta \Theta^2]| \leq M_J |\nabla y_K(\Theta)[\Delta \Theta^1]| |\nabla y_K(\Theta)[\Delta \Theta^2]| + L_J |\nabla^2 y_K(\Theta)[\Delta \Theta^1, \Delta \Theta^2]|.$$

Therefore, to prove (12), it suffices to bound $\nabla y_K(\Theta)[\Delta \Theta]$ and $\nabla^2 y_K(\Theta)[\Delta \Theta^1, \Delta \Theta^2]$ uniformly over $\Theta \in \Omega_C$ with $\|\Delta \Theta\|_{\text{block}} \leq 1$ and $\|\Delta \Theta^1\|_{\text{block}}, \|\Delta \Theta^2\|_{\text{block}} \leq 1$. The first-order term $\nabla y_K(\Theta)[\Delta \Theta]$ already admits a width-independent bound from Theorem 1. Hence, it remains to bound the second-order directional derivative.

To proceed, fix any directions $\Delta \Theta^1 = (\Delta \mathbf{W}_{1:K}^1, \Delta \mathbf{b}_{1:K}^1)$ and $\Delta \Theta^2 = (\Delta \mathbf{W}_{1:K}^2, \Delta \mathbf{b}_{1:K}^2)$ with $\|\Delta \Theta^1\|_{\text{block}} \leq 1$ and $\|\Delta \Theta^2\|_{\text{block}} \leq 1$. For each $i = 1, \dots, K$, let $\Sigma_i := \text{diag}(\sigma'(z_i))$ and $\Gamma_i := \text{diag}(\sigma''(z_i))$ so that $\|\Sigma_i\|_{\infty} \leq L_{\sigma}$ and $\|\Gamma_i\|_{\infty} \leq M_{\sigma}$. For $1 \leq j, \ell \leq i \leq K$, we introduce the following shorthand notations for the first- and second-order directional derivatives:

$$\begin{aligned} \Lambda_{i,j}^{\mathbf{W}^1} &:= \nabla_{\mathbf{w}_j \mathbf{y}_i} [\Delta \mathbf{W}_j^1], & \Lambda_{i,j}^{\mathbf{b}^1} &:= \nabla_{\mathbf{b}_j \mathbf{y}_i} [\Delta \mathbf{b}_j^1], \\ \Lambda_{i,j}^{\mathbf{W}^2} &:= \nabla_{\mathbf{w}_j \mathbf{y}_i} [\Delta \mathbf{W}_j^2], & \Lambda_{i,j}^{\mathbf{b}^2} &:= \nabla_{\mathbf{b}_j \mathbf{y}_i} [\Delta \mathbf{b}_j^2], \\ \Xi_{i,j,\ell}^{\mathbf{W}} &:= \nabla_{\mathbf{w}_j, \mathbf{w}_\ell}^2 \mathbf{y}_i [\Delta \mathbf{W}_j^1, \Delta \mathbf{W}_\ell^2], & \Xi_{i,j,\ell}^{\mathbf{b}} &:= \nabla_{\mathbf{b}_j, \mathbf{b}_\ell}^2 \mathbf{y}_i [\Delta \mathbf{b}_j^1, \Delta \mathbf{b}_\ell^2], \\ \Xi_{i,j,\ell}^{\mathbf{W}, \mathbf{b}} &:= \nabla_{\mathbf{w}_j, \mathbf{b}_\ell}^2 \mathbf{y}_i [\Delta \mathbf{W}_j^1, \Delta \mathbf{b}_\ell^2]. \end{aligned}$$

Since the first-order derivatives have already been computed in (8), we next compute the second-order directional derivatives by differentiating (8) once more and applying the second-order chain rule. Recall that $\mathbf{y}_0 = \mathbf{x}$. For any parameter perturbations $\Delta \Theta^1, \Delta \Theta^2$, and for each $i = 1, \dots, K$, we have

$$\nabla^2 \mathbf{y}_i(\Theta)[\Delta \Theta^1, \Delta \Theta^2] = \Gamma_i \left(\nabla \mathbf{z}_i(\Theta)[\Delta \Theta^1] \odot \nabla \mathbf{z}_i(\Theta)[\Delta \Theta^2] \right) + \Sigma_i \nabla^2 \mathbf{z}_i(\Theta)[\Delta \Theta^1, \Delta \Theta^2],$$

where $\mathbf{z}_i = \mathbf{W}_i \mathbf{y}_{i-1} + \mathbf{b}_i$, and

$$\nabla \mathbf{z}_i(\Theta)[\Delta \Theta] = \Delta \mathbf{W}_i \mathbf{y}_{i-1} + \mathbf{W}_i \nabla \mathbf{y}_{i-1}(\Theta)[\Delta \Theta] + \Delta \mathbf{b}_i,$$

$$\begin{aligned} &\nabla^2 \mathbf{z}_i(\Theta)[\Delta \Theta^1, \Delta \Theta^2] \\ &= \Delta \mathbf{W}_i^1 \nabla \mathbf{y}_{i-1}(\Theta)[\Delta \Theta^2] + \Delta \mathbf{W}_i^2 \nabla \mathbf{y}_{i-1}(\Theta)[\Delta \Theta^1] + \mathbf{W}_i \nabla^2 \mathbf{y}_{i-1}(\Theta)[\Delta \Theta^1, \Delta \Theta^2]. \end{aligned}$$

We decompose the second-order directional derivative layerwise as

$$\begin{aligned} \nabla^2 \mathbf{y}_K(\Theta)[\Delta \Theta^1, \Delta \Theta^2] &= \sum_{1 \leq j, \ell \leq K} \left(\nabla_{\mathbf{w}_j, \mathbf{w}_\ell}^2 \mathbf{y}_K [\Delta \mathbf{W}_j^1, \Delta \mathbf{W}_\ell^2] + \nabla_{\mathbf{w}_j, \mathbf{b}_\ell}^2 \mathbf{y}_K [\Delta \mathbf{W}_j^1, \Delta \mathbf{b}_\ell^2] \right) \\ &\quad + \sum_{1 \leq j, \ell \leq K} \left(\nabla_{\mathbf{b}_j, \mathbf{w}_\ell}^2 \mathbf{y}_K [\Delta \mathbf{b}_j^1, \Delta \mathbf{W}_\ell^2] + \nabla_{\mathbf{b}_j, \mathbf{b}_\ell}^2 \mathbf{y}_K [\Delta \mathbf{b}_j^1, \Delta \mathbf{b}_\ell^2] \right). \end{aligned}$$

The two mixed terms $\nabla_{\mathbf{w}_j, \mathbf{b}_\ell}^2 \mathbf{y}_K[\cdot, \cdot]$ and $\nabla_{\mathbf{b}_j, \mathbf{w}_\ell}^2 \mathbf{y}_K[\cdot, \cdot]$ can be treated analogously and therefore admit the same bound. Hence, it suffices to establish bounds for the three types of terms introduced above. We now specialize the chain-rule identity to layerwise perturbations to derive recursion formulas for the second-order quantities. In what follows, we only derive recursion formulas for $\Xi_{i,j,\ell}^{\mathbf{W}}$ and $\Xi_{i,j,\ell}^{\mathbf{b}}$ with $j \leq \ell$. The remaining cases $j > \ell$ follow by symmetry of the Hessian.

$$\Xi_{i,j,\ell}^{\mathbf{W}} = \begin{cases} \Gamma_i \left((\Delta \mathbf{W}_j^1 \mathbf{y}_{i-1}) \odot (\Delta \mathbf{W}_\ell^2 \mathbf{y}_{i-1}) \right), & j = \ell = i, \\ \Gamma_i \left((\mathbf{W}_i \Lambda_{i-1,j}^{\mathbf{W}^1}) \odot (\Delta \mathbf{W}_\ell^2 \mathbf{y}_{i-1}) \right) + \Sigma_i \Delta \mathbf{W}_\ell^2 \Lambda_{i-1,j}^{\mathbf{W}^1}, & j < \ell = i, \\ \Gamma_i \left((\mathbf{W}_i \Lambda_{i-1,j}^{\mathbf{W}^1}) \odot (\mathbf{W}_i \Lambda_{i-1,\ell}^{\mathbf{W}^2}) \right) + \Sigma_i \mathbf{W}_i \Xi_{i-1,j,\ell}^{\mathbf{W}}, & \ell < i. \end{cases}$$

$$\Xi_{i,j,\ell}^{\mathbf{b}} = \begin{cases} \Gamma_i \left(\Delta \mathbf{b}_j^1 \odot \Delta \mathbf{b}_\ell^2 \right), & j = \ell = i, \\ \Gamma_i \left((\mathbf{W}_i \Lambda_{i-1,j}^{\mathbf{b}^1}) \odot \Delta \mathbf{b}_\ell^2 \right), & j < \ell = i, \\ \Gamma_i \left((\mathbf{W}_i \Lambda_{i-1,j}^{\mathbf{b}^1}) \odot (\mathbf{W}_i \Lambda_{i-1,\ell}^{\mathbf{b}^2}) \right) + \Sigma_i \mathbf{W}_i \Xi_{i-1,j,\ell}^{\mathbf{b}}, & \ell < i. \end{cases}$$

$$\Xi_{i,j,\ell}^{\mathbf{W},\mathbf{b}} = \begin{cases} \Gamma_i \left((\Delta \mathbf{W}_j^1 \mathbf{y}_{i-1}) \odot \Delta \mathbf{b}_\ell^2 \right), & j = \ell = i, \\ \Gamma_i \left((\mathbf{W}_i \Lambda_{i-1,j}^{\mathbf{W}^1}) \odot \Delta \mathbf{b}_\ell^2 \right), & j < \ell = i, \\ \Gamma_i \left((\Delta \mathbf{W}_j^1 \mathbf{y}_{i-1}) \odot (\mathbf{W}_i \Lambda_{i-1,\ell}^{\mathbf{b}^2}) \right) + \Sigma_i \Delta \mathbf{W}_j^1 \Lambda_{i-1,\ell}^{\mathbf{b}^2}, & \ell < j = i, \\ \Gamma_i \left((\mathbf{W}_i \Lambda_{i-1,j}^{\mathbf{W}^1}) \odot (\mathbf{W}_i \Lambda_{i-1,\ell}^{\mathbf{b}^2}) \right) + \Sigma_i \mathbf{W}_i \Xi_{i-1,j,\ell}^{\mathbf{W},\mathbf{b}}, & \ell, j < i. \end{cases}$$

We now bound these quantities case by case.

Case 1: $j = \ell = i$. For $2 \leq i \leq K-1$, we have

$$\begin{aligned} & \left\| \Xi_{i,i,i}^{\mathbf{W}} \right\|_{(p,\text{mean})} \\ & \leq \|\Gamma_i\|_\infty \left\| (\Delta \mathbf{W}_i^1 \mathbf{y}_{i-1}) \odot (\Delta \mathbf{W}_i^2 \mathbf{y}_{i-1}) \right\|_{(p,\text{mean})} \\ & \leq M_\sigma w^{\max(0, \frac{2}{q} - \frac{1}{p})} \left\| \Delta \mathbf{W}_i^1 \mathbf{y}_{i-1} \right\|_{(q,\text{mean})} \left\| \Delta \mathbf{W}_i^2 \mathbf{y}_{i-1} \right\|_{(q,\text{mean})} \\ & \leq M_\sigma w^{\max(0, \frac{2}{q} - \frac{1}{p})} \left\| \Delta \mathbf{W}_i^1 \right\|_{(p,\text{mean}) \rightarrow (q,\text{mean})} \left\| \mathbf{y}_{i-1} \right\|_{(p,\text{mean})} \left\| \Delta \mathbf{W}_i^2 \right\|_{(p,\text{mean}) \rightarrow (q,\text{mean})} \left\| \mathbf{y}_{i-1} \right\|_{(p,\text{mean})} \\ & \leq M_\sigma w^{\max(0, \frac{2}{q} - \frac{1}{p})} \left\| \mathbf{y}_{i-1} \right\|_{(q,\text{mean})}^2 \\ & \leq M_\sigma 2^{2i-2} L_\sigma^{2i-2} C^{2i} w^{\max(0, \frac{2}{q} - \frac{1}{p})}, \end{aligned}$$

where the second inequality follows from Lemma 4, the fourth one is due to Fact 2, and the last one is from (7). Similarly, we have

$$\left\| \Xi_{i,i,i}^{\mathbf{b}} \right\|_{(p,\text{mean})} \leq \|\Gamma_i\|_\infty \left\| \Delta \mathbf{b}_i^1 \odot \Delta \mathbf{b}_i^2 \right\|_\infty \leq M_\sigma, \text{ and}$$

$$\begin{aligned} \left\| \Xi_{i,i,i}^{\mathbf{W},\mathbf{b}} \right\|_{(p,\text{mean})} & \leq \|\Gamma_i\|_\infty \left\| (\Delta \mathbf{W}_i^1 \mathbf{y}_{i-1}) \odot \Delta \mathbf{b}_i^2 \right\|_{(p,\text{mean})} \\ & \leq M_\sigma \left\| \Delta \mathbf{b}_i^2 \right\|_\infty \left\| \Delta \mathbf{W}_i^1 \mathbf{y}_{i-1} \right\|_{(p,\text{mean})} \\ & \leq M_\sigma \left\| \Delta \mathbf{W}_i^1 \right\|_{(p,\text{mean}) \rightarrow (q,\text{mean})} \left\| \mathbf{y}_{i-1} \right\|_{(p,\text{mean})} \\ & \leq M_\sigma \left\| \Delta \mathbf{W}_i^1 \right\|_{(p,\text{mean}) \rightarrow (q,\text{mean})} \left\| \mathbf{y}_{i-1} \right\|_{(q,\text{mean})} \leq M_\sigma 2^{i-1} L_\sigma^{i-1} C^i. \end{aligned}$$

Similarly, for the boundary layers $i = 1$ and $i = K$, by replacing $\|\cdot\|_{(p,\text{mean}) \rightarrow (q,\text{mean})}$ with $\|\cdot\|_{1 \rightarrow (q,\text{mean})}$ and $\|\cdot\|_{(p,\text{mean}) \rightarrow \infty}$ respectively, we obtain the following bounds,

$$\begin{aligned} \left\| \Xi_{1,1,1}^{\mathbf{W}} \right\|_{(p,\text{mean})} & \leq M_\sigma C^2 w^{\max(0, \frac{2}{q} - \frac{1}{p})}, \\ \left| \Xi_{K,K,K}^{\mathbf{W}} \right| & \leq M_\sigma 2^{2K-2} L_\sigma^{2K-2} C^{2K} w^{\max(0, \frac{2}{q} - \frac{1}{p})}, \\ \left\| \Xi_{1,1,1}^{\mathbf{b}} \right\|_{(p,\text{mean})} & \leq \left\| \Xi_{1,1,1}^{\mathbf{b}} \right\|_\infty \leq \|\Gamma_1\|_\infty \left\| \Delta \mathbf{b}_1^1 \odot \Delta \mathbf{b}_1^2 \right\|_\infty \leq M_\sigma, \end{aligned}$$

$$\begin{aligned}
\left| \Xi_{K,K,K}^b \right| &\leq \|\Gamma_K\|_\infty \|\Delta \mathbf{b}_K^1 \odot \Delta \mathbf{b}_K^2\|_\infty \leq M_\sigma, \\
\left\| \Xi_{1,1,1}^{\mathbf{W},b} \right\|_{(p,\text{mean})} &\leq \|\Gamma_1\|_\infty \|(\Delta \mathbf{W}_1^1 \mathbf{y}_0) \odot \Delta \mathbf{b}_1^2\|_\infty \leq M_\sigma \sqrt{d} C, \\
\left| \Xi_{K,K,K}^{\mathbf{W},b} \right| &\leq \|\Gamma_K\|_\infty \|(\Delta \mathbf{W}_K^1 \mathbf{y}_{K-1}) \odot \Delta \mathbf{b}_K^2\|_\infty \leq M_\sigma 2^{K-1} L_\sigma^{K-1} C^K.
\end{aligned}$$

Case 2: $\min\{j, \ell\} < \max\{j, \ell\} = i$. For $2 \leq i \leq K-1$, we first bound the weight–weight and bias–bias blocks for $j < \ell = i$. The remaining case $\ell < j = 1$ follows by symmetry. For the mixed blocks, both boundary configurations $\Xi_{i,j,i}^{\mathbf{W},b}$ ($j < \ell = i$) and $\Xi_{i,i,\ell}^{\mathbf{W},b}$ ($\ell < j = i$) appear and will be bounded separately.

$$\begin{aligned}
&\left\| \Xi_{i,j,i}^{\mathbf{W}} \right\|_{(p,\text{mean})} \\
&= \left\| \Gamma_i \left((\mathbf{W}_i \Lambda_{i-1,j}^{\mathbf{W}^1}) \odot (\Delta \mathbf{W}_i^2 \mathbf{y}_{i-1}) \right) + \Sigma_i \Delta \mathbf{W}_i^2 \Lambda_{i-1,j}^{\mathbf{W}^1} \right\|_{(p,\text{mean})} \\
&\leq \|\Gamma_i\|_\infty \left\| \left((\mathbf{W}_i \Lambda_{i-1,j}^{\mathbf{W}^1}) \odot (\Delta \mathbf{W}_i^2 \mathbf{y}_{i-1}) \right) \right\|_{(p,\text{mean})} + \left\| \Sigma_i \Delta \mathbf{W}_i^2 \Lambda_{i-1,j}^{\mathbf{W}^1} \right\|_{(p,\text{mean})} \\
&\leq M_\sigma W^{\max(0, \frac{2}{q} - \frac{1}{p})} \left\| \mathbf{W}_i \Lambda_{i-1,j}^{\mathbf{W}^1} \right\|_{(q,\text{mean})} \left\| \Delta \mathbf{W}_i^2 \mathbf{y}_{i-1} \right\|_{(q,\text{mean})} \\
&\quad + L_\sigma \left\| \Delta \mathbf{W}_i^2 \right\|_{(p,\text{mean}) \rightarrow (q,\text{mean})} \left\| \Lambda_{i-1,j}^{\mathbf{W}^1} \right\|_{(p,\text{mean})} \\
&\leq M_\sigma W^{\max(0, \frac{2}{q} - \frac{1}{p})} \left\| \mathbf{W}_i \right\|_{(p,\text{mean}) \rightarrow (q,\text{mean})} \left\| \Lambda_{i-1,j}^{\mathbf{W}^1} \right\|_{(p,\text{mean})} \left\| \Delta \mathbf{W}_i^2 \right\|_{(p,\text{mean}) \rightarrow (q,\text{mean})} \|\mathbf{y}_{i-1}\|_{(q,\text{mean})} \\
&\quad + L_\sigma \left\| \Delta \mathbf{W}_i^2 \right\|_{(p,\text{mean}) \rightarrow (q,\text{mean})} \left\| \Lambda_{i-1,j}^{\mathbf{W}^1} \right\|_{(p,\text{mean})} \\
&\leq M_\sigma W^{\max(0, \frac{2}{q} - \frac{1}{p})} C \left\| \Lambda_{i-1,j}^{\mathbf{W}^1} \right\|_{(p,\text{mean})} \|\mathbf{y}_{i-1}\|_{(q,\text{mean})} + L_\sigma \left\| \Lambda_{i-1,j}^{\mathbf{W}^1} \right\|_{(p,\text{mean})} \\
&\leq M_\sigma W^{\max(0, \frac{2}{q} - \frac{1}{p})} 2^{2i-3} L_\sigma^{2i-2} C^{2i} + 2^{i-2} L_\sigma^i C^{i-1},
\end{aligned}$$

where the second inequality follows from Lemma 4 and the definition of the operator norm, and the last one is from (7) and (10). Similarly, we have

$$\begin{aligned}
\left\| \Xi_{i,j,i}^b \right\|_{(p,\text{mean})} &\leq \|\Gamma_i\|_\infty \left\| (\mathbf{W}_i \Lambda_{i-1,j}^{\mathbf{b}^1}) \odot \Delta \mathbf{b}_i^2 \right\|_{(p,\text{mean})} \\
&\leq M_\sigma W^{\max(0, \frac{2}{q} - \frac{1}{p})} \left\| \mathbf{W}_i \right\|_{(p,\text{mean}) \rightarrow (q,\text{mean})} \left\| \Lambda_{i-1,j}^{\mathbf{b}^1} \right\|_{(p,\text{mean})} \|\Delta \mathbf{b}_i^2\|_\infty \\
&\leq M_\sigma W^{\max(0, \frac{2}{q} - \frac{1}{p})} L_\sigma^{i-1} C^{i-1},
\end{aligned}$$

where the last inequality follows from (11). Then, we continue to bound two cross terms:

$$\begin{aligned}
\left\| \Xi_{i,j,i}^{\mathbf{W},b} \right\|_{(p,\text{mean})} &= \left\| \Gamma_i \left((\mathbf{W}_i \Lambda_{i-1,j}^{\mathbf{W}^1}) \odot \Delta \mathbf{b}_i^2 \right) \right\|_{(p,\text{mean})} \\
&\leq \|\Gamma_i\|_\infty \left\| \mathbf{W}_i \Lambda_{i-1,j}^{\mathbf{W}^1} \right\|_{(q,\text{mean})} \|\Delta \mathbf{b}_i^2\|_\infty \\
&\leq M_\sigma \left\| \mathbf{W}_i \right\|_{(p,\text{mean}) \rightarrow (q,\text{mean})} \left\| \Lambda_{i-1,j}^{\mathbf{W}^1} \right\|_{(p,\text{mean})} \leq M_\sigma 2^{i-2} L_\sigma^{i-1} C^i, \quad (j < \ell = i)
\end{aligned}$$

$$\begin{aligned}
&\left\| \Xi_{i,i,\ell}^{\mathbf{W},b} \right\|_{(p,\text{mean})} \\
&= \left\| \Gamma_i \left((\Delta \mathbf{W}_i \mathbf{y}_{i-1}) \odot (\mathbf{W}_i \Lambda_{i-1,\ell}^{\mathbf{b}^2}) \right) + \Sigma_i \Delta \mathbf{W}_i^1 \Lambda_{i-1,\ell}^{\mathbf{b}^2} \right\|_{(p,\text{mean})} \\
&\leq \|\Gamma_i\|_\infty \left\| (\Delta \mathbf{W}_i \mathbf{y}_{i-1}) \odot (\mathbf{W}_i \Lambda_{i-1,\ell}^{\mathbf{b}^2}) \right\|_{(p,\text{mean})} + \left\| \Sigma_i \Delta \mathbf{W}_i^1 \Lambda_{i-1,\ell}^{\mathbf{b}^2} \right\|_{(p,\text{mean})} \\
&\leq M_\sigma W^{\max(0, \frac{2}{q} - \frac{1}{p})} \left\| \Delta \mathbf{W}_i \right\|_{(p,\text{mean}) \rightarrow (q,\text{mean})} \|\mathbf{y}_{i-1}\|_{(p,\text{mean})} \left\| \mathbf{W}_i \right\|_{(p,\text{mean}) \rightarrow (q,\text{mean})} \left\| \Lambda_{i-1,\ell}^{\mathbf{b}^2} \right\|_{(p,\text{mean})} \\
&\quad + L_\sigma \left\| \Delta \mathbf{W}_i^1 \right\|_{(p,\text{mean}) \rightarrow (q,\text{mean})} \left\| \Lambda_{i-1,\ell}^{\mathbf{b}^2} \right\|_{(p,\text{mean})}
\end{aligned}$$

$$\begin{aligned}
&\leq M_{\sigma} w^{\max\left(0, \frac{2}{q} - \frac{1}{p}\right)} C \|y_{i-1}\|_{(q, \text{mean})} \left\| \Lambda_{i-1, \ell}^{\mathbf{b}^2} \right\|_{(p, \text{mean})} + L_{\sigma} \left\| \Lambda_{i-1, \ell}^{\mathbf{b}^2} \right\|_{(p, \text{mean})} \\
&\leq M_{\sigma} w^{\max\left(0, \frac{2}{q} - \frac{1}{p}\right)} 2^{i-1} L_{\sigma}^{2i-2} C^{2i-1} + L_{\sigma}^i C^{i-2}, \quad (\ell < j = i).
\end{aligned}$$

Case 3: $\max\{j, \ell\} < i < K$. Similar with **Case 2**, WLOG, we assume $j \leq \ell$.

$$\begin{aligned}
\left\| \Xi_{i,j,\ell}^{\mathbf{W}} \right\|_{(p, \text{mean})} &= \left\| \Gamma_i \left((\mathbf{W}_i \Lambda_{i-1,j}^{\mathbf{W}^1}) \odot (\mathbf{W}_i \Lambda_{i-1,\ell}^{\mathbf{W}^2}) \right) + \Sigma_i \mathbf{W}_i \Xi_{i-1,j,\ell}^{\mathbf{W}} \right\|_{(p, \text{mean})} \\
&\leq M_{\sigma} w^{\max\left(0, \frac{2}{q} - \frac{1}{p}\right)} \left\| \mathbf{W}_i \Lambda_{i-1,j}^{\mathbf{W}^1} \right\|_{(q, \text{mean})} \left\| \mathbf{W}_i \Lambda_{i-1,\ell}^{\mathbf{W}^2} \right\|_{(q, \text{mean})} \\
&\quad + L_{\sigma} \|\mathbf{W}_i\|_{(p, \text{mean}) \rightarrow (q, \text{mean})} \left\| \Xi_{i-1,j,\ell}^{\mathbf{W}} \right\|_{(p, \text{mean})} \\
&\leq M_{\sigma} w^{\max\left(0, \frac{2}{q} - \frac{1}{p}\right)} \|\mathbf{W}_i\|_{(p, \text{mean}) \rightarrow (q, \text{mean})}^2 \left\| \Lambda_{i-1,j}^{\mathbf{W}^1} \right\|_{(p, \text{mean})} \left\| \Lambda_{i-1,\ell}^{\mathbf{W}^2} \right\|_{(p, \text{mean})} \\
&\quad + L_{\sigma} \|\mathbf{W}_i\|_{(p, \text{mean}) \rightarrow (q, \text{mean})} \left\| \Xi_{i-1,j,\ell}^{\mathbf{W}} \right\|_{(p, \text{mean})} \\
&\leq M_{\sigma} w^{\max\left(0, \frac{2}{q} - \frac{1}{p}\right)} 2^{2i-4} L_{\sigma}^{2i-2} C^{2i} + L_{\sigma} C \left\| \Xi_{i-1,j,\ell}^{\mathbf{W}} \right\|_{(p, \text{mean})}.
\end{aligned}$$

Combining the bounds from Cases 1–2 and unrolling the above recursion, we obtain

$$\left\| \Xi_{i,j,\ell}^{\mathbf{W}} \right\|_{(p, \text{mean})} \lesssim w^{\max\left(0, \frac{2}{q} - \frac{1}{p}\right)},$$

where the hidden constant depends only on C , K , L_{σ} , and M_{σ} , but is independent of the layer widths. Similarly, we have

$$\begin{aligned}
&\left\| \Xi_{i,j,\ell}^{\mathbf{b}} \right\|_{(p, \text{mean})} \\
&= \left\| \Gamma_i \left((\mathbf{W}_i \Lambda_{i-1,j}^{\mathbf{b}^1}) \odot (\mathbf{W}_i \Lambda_{i-1,\ell}^{\mathbf{b}^2}) \right) + \Sigma_i \mathbf{W}_i \Xi_{i-1,j,\ell}^{\mathbf{b}} \right\|_{(p, \text{mean})} \\
&\leq M_{\sigma} w^{\max\left(0, \frac{2}{q} - \frac{1}{p}\right)} \left\| \mathbf{W}_i \Lambda_{i-1,j}^{\mathbf{b}^1} \right\|_{(q, \text{mean})} \left\| \mathbf{W}_i \Lambda_{i-1,\ell}^{\mathbf{b}^2} \right\|_{(q, \text{mean})} + L_{\sigma} \left\| \mathbf{W}_i \Xi_{i-1,j,\ell}^{\mathbf{b}} \right\|_{(q, \text{mean})} \\
&\leq M_{\sigma} w^{\max\left(0, \frac{2}{q} - \frac{1}{p}\right)} \|\mathbf{W}_i\|_{(p, \text{mean}) \rightarrow (q, \text{mean})}^2 \left\| \Lambda_{i-1,j}^{\mathbf{b}^1} \right\|_{(p, \text{mean})} \left\| \Lambda_{i-1,\ell}^{\mathbf{b}^2} \right\|_{(p, \text{mean})} \\
&\quad + L_{\sigma} \|\mathbf{W}_i\|_{(p, \text{mean}) \rightarrow (q, \text{mean})} \left\| \Xi_{i-1,j,\ell}^{\mathbf{b}} \right\|_{(p, \text{mean})} \\
&\leq M_{\sigma} w^{\max\left(0, \frac{2}{q} - \frac{1}{p}\right)} (L_{\sigma} C)^{2i-2} + L_{\sigma} C \left\| \Xi_{i-1,j,\ell}^{\mathbf{b}} \right\|_{(p, \text{mean})} \lesssim w^{\max\left(0, \frac{2}{q} - \frac{1}{p}\right)}.
\end{aligned}$$

Finally, for $\Xi_{i,j,\ell}^{\mathbf{W}, \mathbf{b}}$, we have

$$\begin{aligned}
\left\| \Xi_{i,j,\ell}^{\mathbf{W}, \mathbf{b}} \right\|_{(p, \text{mean})} &= \left\| \Gamma_i \left((\mathbf{W}_i \Lambda_{i-1,j}^{\mathbf{W}^1}) \odot (\mathbf{W}_i \Lambda_{i-1,\ell}^{\mathbf{b}^2}) \right) + \Sigma_i \mathbf{W}_i \Xi_{i-1,j,\ell}^{\mathbf{W}, \mathbf{b}} \right\|_{(p, \text{mean})} \\
&\leq M_{\sigma} w^{\max\left(0, \frac{2}{q} - \frac{1}{p}\right)} \left\| \mathbf{W}_i \Lambda_{i-1,j}^{\mathbf{W}^1} \right\|_{(q, \text{mean})} \left\| \mathbf{W}_i \Lambda_{i-1,\ell}^{\mathbf{b}^2} \right\|_{(q, \text{mean})} \\
&\quad + L_{\sigma} \|\mathbf{W}_i\|_{(p, \text{mean}) \rightarrow (q, \text{mean})} \left\| \Xi_{i-1,j,\ell}^{\mathbf{W}, \mathbf{b}} \right\|_{(p, \text{mean})} \\
&\leq M_{\sigma} w^{\max\left(0, \frac{2}{q} - \frac{1}{p}\right)} \|\mathbf{W}_i\|_{(p, \text{mean}) \rightarrow (q, \text{mean})}^2 \left\| \Lambda_{i-1,j}^{\mathbf{W}^1} \right\|_{(p, \text{mean})} \left\| \Lambda_{i-1,\ell}^{\mathbf{b}^2} \right\|_{(p, \text{mean})} \\
&\quad + L_{\sigma} \|\mathbf{W}_i\|_{(p, \text{mean}) \rightarrow (q, \text{mean})} \left\| \Xi_{i-1,j,\ell}^{\mathbf{W}, \mathbf{b}} \right\|_{(p, \text{mean})} \\
&\leq M_{\sigma} w^{\max\left(0, \frac{2}{q} - \frac{1}{p}\right)} 2^{i-2} L_{\sigma}^{2i-2} C^{2i-1} + L_{\sigma} C \left\| \Xi_{i-1,j,\ell}^{\mathbf{W}, \mathbf{b}} \right\|_{(p, \text{mean})} \lesssim w^{\max\left(0, \frac{2}{q} - \frac{1}{p}\right)}.
\end{aligned}$$

Case 4: $\max\{j, \ell\} < i = K$. WLOG, we assume $j \leq \ell$. With the similar computation as **Case 3**, we have

$$\left| \Xi_{K,j,\ell}^{\mathbf{W}} \right| = \left| \Gamma_K \left((\mathbf{W}_K \Lambda_{K-1,j}^{\mathbf{W}^1}) \cdot (\mathbf{W}_K \Lambda_{K-1,\ell}^{\mathbf{W}^2}) \right) + \Sigma_K \mathbf{W}_K \Xi_{K-1,j,\ell}^{\mathbf{W}} \right|$$

$$\begin{aligned}
&\leq M_\sigma \left| \mathbf{W}_K \Lambda_{K-1,j}^{\mathbf{W}^1} \right| \left| \mathbf{W}_K \Lambda_{K-1,\ell}^{\mathbf{W}^2} \right| + L_\sigma \|\mathbf{W}_K\|_{(p,\text{mean}) \rightarrow \infty} \left\| \Xi_{K-1,j,\ell}^{\mathbf{W}} \right\|_{(p,\text{mean})} \\
&\leq M_\sigma \|\mathbf{W}_i\|_{(p,\text{mean}) \rightarrow \infty} \left\| \Lambda_{K-1,j}^{\mathbf{W}^1} \right\|_{(p,\text{mean})} \|\mathbf{W}_i\|_{(p,\text{mean}) \rightarrow \infty} \left\| \Lambda_{K-1,\ell}^{\mathbf{W}^2} \right\|_{(p,\text{mean})} \\
&\quad + L_\sigma C \left\| \Xi_{K-1,j,\ell}^{\mathbf{W}} \right\|_{(p,\text{mean})} \lesssim w^{\max(0, \frac{2}{q} - \frac{1}{p})}, \\
\left| \Xi_{K,j,\ell}^{\mathbf{b}} \right| &= \left| \Gamma_K \left((\mathbf{W}_K \Lambda_{K-1,j}^{\mathbf{b}^1}) \cdot (\mathbf{W}_K \Lambda_{K-1,\ell}^{\mathbf{b}^2}) \right) + \Sigma_K \mathbf{W}_K \Xi_{K-1,j,\ell}^{\mathbf{b}} \right| \\
&\leq M_\sigma \left| \mathbf{W}_K \Lambda_{K-1,j}^{\mathbf{b}^1} \right| \left| \mathbf{W}_K \Lambda_{K-1,\ell}^{\mathbf{b}^2} \right| + L_\sigma \|\mathbf{W}_K\|_{(p,\text{mean}) \rightarrow \infty} \left\| \Xi_{K-1,j,\ell}^{\mathbf{b}} \right\|_{(p,\text{mean})} \\
&\leq M_\sigma \|\mathbf{W}_K\|_{(p,\text{mean}) \rightarrow \infty} \left\| \Lambda_{K-1,j}^{\mathbf{b}^1} \right\|_{(p,\text{mean})} \|\mathbf{W}_K\|_{(p,\text{mean}) \rightarrow \infty} \left\| \Lambda_{K-1,\ell}^{\mathbf{b}^2} \right\|_{(p,\text{mean})} \\
&\quad + L_\sigma \|\mathbf{W}_K\|_{(p,\text{mean}) \rightarrow \infty} \left\| \Xi_{K-1,j,\ell}^{\mathbf{b}} \right\|_{(p,\text{mean})} \lesssim w^{\max(0, \frac{2}{q} - \frac{1}{p})}.
\end{aligned}$$

Finally, for $\Xi_{K,j,\ell}^{\mathbf{W},\mathbf{b}}$ and $\Xi_{K,\ell,j}^{\mathbf{W},\mathbf{b}}$, we have

$$\begin{aligned}
\left| \Xi_{K,j,\ell}^{\mathbf{W},\mathbf{b}} \right| &= \left| \Gamma_K \left((\mathbf{W}_K \Lambda_{K-1,j}^{\mathbf{W}^1}) \cdot (\mathbf{W}_K \Lambda_{K-1,\ell}^{\mathbf{b}^2}) \right) + \Sigma_K \mathbf{W}_K \Xi_{K-1,j,\ell}^{\mathbf{W},\mathbf{b}} \right| \\
&\leq M_\sigma \left| \mathbf{W}_K \Lambda_{K-1,j}^{\mathbf{W}^1} \right| \left| \mathbf{W}_K \Lambda_{K-1,\ell}^{\mathbf{b}^2} \right| + L_\sigma \|\mathbf{W}_K\|_{(p,\text{mean}) \rightarrow \infty} \left\| \Xi_{K-1,j,\ell}^{\mathbf{W},\mathbf{b}} \right\|_{(p,\text{mean})} \\
&\leq M_\sigma \|\mathbf{W}_i\|_{(p,\text{mean}) \rightarrow \infty} \left\| \Lambda_{K-1,j}^{\mathbf{W}^1} \right\|_{(p,\text{mean})} \|\mathbf{W}_i\|_{(p,\text{mean}) \rightarrow \infty} \left\| \Lambda_{K-1,\ell}^{\mathbf{b}^2} \right\|_{(p,\text{mean})} \\
&\quad + L_\sigma C \left\| \Xi_{K-1,j,\ell}^{\mathbf{W},\mathbf{b}} \right\|_{(p,\text{mean})} \lesssim w^{\max(0, \frac{2}{q} - \frac{1}{p})}.
\end{aligned}$$

Putting everything together yields the result. \square

Message: While certain operator-norm geometries allow the M -Lipschitz constant to remain well controlled, the behavior of the L -smoothness coefficient can vary significantly:

- **Muon:** Under the $\|\cdot\|_{(2,\text{mean}) \rightarrow (2,\text{mean})}$ geometry, the L -smoothness coefficient scales as $O(\sqrt{\text{width}})$.
- **Width-independent smoothness:** In contrast, width-independent L -smoothness can be achieved under alternative geometries. In particular, the gradient of a neural network admits a width-independent L -smoothness coefficient under the $\|\cdot\|_{(1,\text{mean}) \rightarrow (p,\text{mean})}$ or $\|\cdot\|_{(p,\text{mean}) \rightarrow \infty}$ geometries. As a special case, under the $\|\cdot\|_{(1,\text{mean}) \rightarrow \infty}$ geometry associated with Adam/SignSGD, the L -smoothness coefficient is width-independent.

2.4 MOGA Optimizer

In this subsection, we show that passing from the classical $p \rightarrow q$ geometry to the $(p, \text{mean}) \rightarrow (q, \text{mean})$ geometry amounts to a width-aware rescaling of the learning rate. This follows from the fact that the mean-normalized norm $\|\cdot\|_{(p,\text{mean})}$ differs from the standard ℓ_p norm on \mathbb{R}^d only by a multiplicative factor of $d^{1/p}$. Consequently, the two geometries induce equivalent update directions up to a dimension-dependent scaling, which can be absorbed into the step size. Moreover, we show that the resulting width-aware rescaling coincides exactly with the μP scaling rule of [60] in the special cases of Adam and SignSGD. Precisely, the following equivalence holds.

Fact 3. Let $\mathbf{D} \in \mathbb{R}^{d_{\text{out}} \times d_{\text{in}}}$ and $1 \leq p, q \leq \infty$. Then the operator norms under the mean-normalized geometry satisfy

$$\|\mathbf{D}\|_{(p,\text{mean}) \rightarrow (q,\text{mean})} = \frac{d_{\text{in}}^{1/p}}{d_{\text{out}}^{1/q}} \cdot \|\mathbf{D}\|_{p \rightarrow q}.$$

Consequently, the steepest-ascent directions induced by these norms coincide with those in Proposition 1 up to a width-dependent rescaling factor. In particular,

(i) (*Column-wise update*, $\|\cdot\|_{(1,\text{mean}) \rightarrow (q,\text{mean})}$)

$$\mathbf{D}^\star = \boxed{\frac{d_{\text{out}}^{1/q}}{d_{\text{in}}}} \cdot \text{colnorm}_q(\mathbf{G}).$$

(ii) (*Row-wise update*, $\|\cdot\|_{(p,\text{mean}) \rightarrow \infty}$)

$$\mathbf{D}^\star = \boxed{\frac{1}{d_{\text{in}}^{1/p}}} \cdot \text{rownorm}_p(\mathbf{G}).$$

Proof. Proof of Fact 3. By Definition 1, we have

$$\|\mathbf{D}\|_{(p,\text{mean}) \rightarrow (q,\text{mean})} = \sup_{\mathbf{x} \neq \mathbf{0}} \frac{\|\mathbf{D}\mathbf{x}\|_{(q,\text{mean})}}{\|\mathbf{x}\|_{(p,\text{mean})}} = \frac{d_{\text{in}}^{1/p}}{d_{\text{out}}^{1/q}} \sup_{\mathbf{x} \neq \mathbf{0}} \frac{\|\mathbf{D}\mathbf{x}\|_q}{\|\mathbf{x}\|_p} = \frac{d_{\text{in}}^{1/p}}{d_{\text{out}}^{1/q}} \|\mathbf{D}\|_{p \rightarrow q},$$

which establishes the claimed identities. This completes the proof. \square

The $(p, \text{mean}) \rightarrow (q, \text{mean})$ geometry induces update directions that coincide with those of the classical $p \rightarrow q$ geometry up to width-dependent rescaling factors. These factors, highlighted in Fact 3 (boxed for emphasis), are referred to as MOGA (Matrix Operator Geometry Aware) scaling. Motivated by this observation, we introduce a simple yet general family of optimizers based on this scaling, which we term **MOGA**. Here, we treat all parameters in a block-wise manner. Gradients and momentum variables inherit the same block structure as $\Theta = \{\mathbf{W}_i, \mathbf{b}_i\}_{i=1}^\ell$.

Algorithm 1 MOGA: Matrix-Operator-Geometry-Aware Steepest Descent

Require: Learning rates $\{\eta^t\}_{t \geq 0}$, momentum parameters $\beta_1, \beta_2 \in (0, 1)$, initial parameters Θ^0

- 1: $\mathbf{M}^0 \leftarrow \mathbf{0}$ $\triangleright \mathbf{M}^t$ has the same block structure as Θ^t
- 2: **for** $t = 1, 2, \dots$ **do**
- 3: Sample stochastic gradient: $\mathbf{G} \leftarrow \nabla F(\Theta^{t-1}; \xi)$, $\xi \sim \mathbb{P}$
- 4: Exponential moving average: $\mathbf{M}^t \leftarrow \beta_1 \mathbf{M}^{t-1} + (1 - \beta_1) \mathbf{G}$
- 5: Lookahead (Nesterov-type) momentum: $\tilde{\mathbf{M}}^t \leftarrow \beta_2 \mathbf{M}^{t-1} + (1 - \beta_2) \mathbf{G}$
- 6: **if** Descent under $(1, \text{mean}) \rightarrow (q, \text{mean})$ **then** $\triangleright q \geq 2$
- 7: **for** $i = 1$ to ℓ **do**
- 8: $\mathbf{W}_i^t \leftarrow \mathbf{W}_i^{t-1} - \eta^t \cdot \boxed{\frac{(d_{\text{out}}^i)^{1/q}}{d_{\text{in}}^i}} \cdot \text{colnorm}_q(\tilde{\mathbf{M}}_{\mathbf{W}_i^{t-1}}^t)$
- 9: $\mathbf{b}_i^t \leftarrow \mathbf{b}_i^{t-1} - \eta^t \text{sign}(\tilde{\mathbf{M}}_{\mathbf{b}_i^t}^t)$ \triangleright or steepest descent under (q, mean) norm
- 10: **end for**
- 11: **else if** Descent under $(p, \text{mean}) \rightarrow \infty$ **then**
- 12: **for** $i = 1$ to ℓ **do**
- 13: $\mathbf{W}_i^t \leftarrow \mathbf{W}_i^{t-1} - \eta^t \cdot \boxed{\frac{1}{(d_{\text{in}}^i)^{1/p}}} \cdot \text{rownorm}_p(\tilde{\mathbf{M}}_{\mathbf{W}_i^{t-1}}^t)$
- 14: $\mathbf{b}_i^t \leftarrow \mathbf{b}_i^{t-1} - \eta^t \text{sign}(\tilde{\mathbf{M}}_{\mathbf{b}_i^t}^t)$
- 15: **end for**
- 16: **end if**
- 17: **end for**

The MOGA scaling derived from our analysis also provides a principled explanation for hyperparameter transfer across widths, namely, that appropriately rescaled parameters and learning rates preserve the effective optimization geometry as the network width grows, thereby maintaining width-independent optimization behavior. Consequently, hyperparameters tuned on small proxy networks can be transferred reliably to much wider models. This property is particularly important in modern large-scale pretraining, where hyperparameter tuning is computationally expensive and reliable transfer across model sizes is crucial.

Moreover, MOGA scaling exactly recovers the Maximal Update Parametrization (μP scaling) [59] in the special case of Adam. Importantly, the underlying principles are conceptually distinct: μP is motivated by preserving feature-learning behavior as width grows (e.g., keeping feature-level update magnitudes non-degenerate), whereas

MOGA scaling arises from an optimization-geometry viewpoint, via width-independent Lipschitz and smoothness control under mean-normalized operator norms. Nevertheless, both lead to the hyperparameter transfer phenomenon observed in practice. The original μP work primarily provided a parametrization rule motivated by feature-learning considerations, without a formal theoretical analysis. Later, the work of [61] proposes a spectral condition requiring the update direction to have spectral norm $\sqrt{\frac{d_{\text{in}}}{d_{\text{out}}}}$, which recovers the μP scaling for SGD. From the perspective of our operator-geometry framework, this spectral condition is equivalent to requiring that the update direction has a width-independent $\|\cdot\|_{(2,\text{mean})\text{arrow}(2,\text{mean})}$ norm. We first verify that MOGA scaling for Adam/SignSGD satisfies the spectral condition of [61]. Fact 2 implies that $\|\cdot\|_{(1,\text{mean})\text{arrow}\infty} \leq \|\cdot\|_{(2,\text{mean})\text{arrow}(2,\text{mean})}$. Therefore, any update direction normalized to unit $\|\cdot\|_{(1,\text{mean})\text{arrow}\infty}$ norm automatically has a width-independent $\|\cdot\|_{(2,\text{mean})\text{arrow}(2,\text{mean})}$ norm, and hence satisfies the spectral condition.

Nevertheless, MOGA scaling also admits regimes where updates remain stable even when the spectral condition is violated. To illustrate this, consider the $(3, \text{mean}) \rightarrow \infty$ operator norm and the rank-one matrix $\mathbf{D} \in \mathbb{R}^{d \times d}$ defined by $\mathbf{D}_{i,1} = d^{-1/3}$ and $\mathbf{D}_{i,j} = 0$ when $j \neq 1$. It is straightforward to verify that $\|\mathbf{D}\|_{(3,\text{mean}) \rightarrow \infty} = 1$. In contrast, its spectral norm satisfies $\|\mathbf{D}\|_{(2,\text{mean}) \rightarrow (2,\text{mean})} = d^{1/6}$, which grows with d and therefore violates the spectral condition. Empirically, as demonstrated in Figure 3 with $p = 3$, the optimal learning rate of MOGA with row normalization remains invariant from GPT-2 Small to GPT-XL, indicating that the optimization dynamics remain stable across widths. This example shows that hyperparameter transfer in practice can arise even outside μP scaling developed through the spectral condition, highlighting the effectiveness of the proposed MOGA scaling.

Message: Under the $(p, \text{mean}) \rightarrow (q, \text{mean})$ geometry, we derive a width-aware *MOGA* scaling rule that applies to a broad family of optimizers. In particular, several commonly used methods arise as special cases:

Optimizer	Geometry	Lr scaling	Remark
Adam / SignSGD	$(1, \text{mean}) \rightarrow \infty$	$1/d_{\text{in}}$	Recovers μP scaling [60]
Column Normalization	$(1, \text{mean}) \rightarrow (q, \text{mean})$	$d_{\text{out}}^{1/q}/d_{\text{in}}$	$q \geq 2$
Row Normalization	$(p, \text{mean}) \rightarrow \infty$	$d_{\text{in}}^{-1/p}$	
Muon	$(2, \text{mean}) \rightarrow (2, \text{mean})$	$\frac{\sqrt{d_{\text{in}}/d_{\text{out}}}}{\sqrt{\max\{d_{\text{out}}, d_{\text{in}}\}}}$	Two controversial learning-rate rules

Remark 4 (Learning Rate Scaling of Muon). *The learning-rate scaling of Muon remains unsettled in the literature, with different prescriptions arising from distinct theoretical viewpoints. (i) Several works [61, 39] interpret Muon as a steepest-descent method under the $(2, \text{mean}) \rightarrow (2, \text{mean})$ operator geometry. Under this perspective, the scaling $\sqrt{d_{\text{in}}/d_{\text{out}}}$ follows directly from the width-independent Lipschitz bound established in Theorem 1, and the width-invariant MOGA scaling rule derived here. (ii) In contrast, large-scale industrial implementations [31] adopt the heuristic prescription $\eta_{\text{Muon}} = \sqrt{\max\{d_{\text{out}}, d_{\text{in}}\}} \eta_{\text{AdamW}}$, where η_{AdamW} denotes the tuned AdamW learning rate. Tensor-program analyses [60] suggest that $\eta_{\text{AdamW}} = \Theta(1/w)$ as the network width w varies, implying that the above rule corresponds to $\eta_{\text{Muon}} = \Theta(1/\sqrt{w})$. This scaling matches the worst-case L -smoothness growth predicted by Theorem 2 under the $(2, \text{mean}) \rightarrow (2, \text{mean})$ geometry. (iii) We hypothesize that these two scalings correspond to different training regimes. Near random initialization, the factor $\sqrt{d_{\text{in}}/d_{\text{out}}}$ helps maintain width-independent Lipschitz control of the loss, whereas the worst-case L -smooth behavior becomes more relevant during later stages of training. This stage-dependent mismatch in step-size scaling may constitute a potential limitation of Muon. In contrast, the MOGA optimizer proposed in this paper derives its scaling directly from the underlying operator geometry, and therefore does not exhibit such regime-dependent inconsistencies.*

3 Generalization to Transformer

We extend the scaling framework developed for feedforward networks in Section 2 to Transformer architectures. In particular, we consider a standard Transformer block and specify, for each parameter matrix, the normalization and parametrization induced by Algorithm 1.

Throughout this section, we adopt the $(p, \text{mean}) \rightarrow (q, \text{mean})$ operator-norm geometry introduced in Section 2. For most weight matrices in the Transformer block, the scaling rules follow directly from the same geometric principle. Vector parameters and a few special weight matrices require slightly different treatment, which we discuss in detail below.

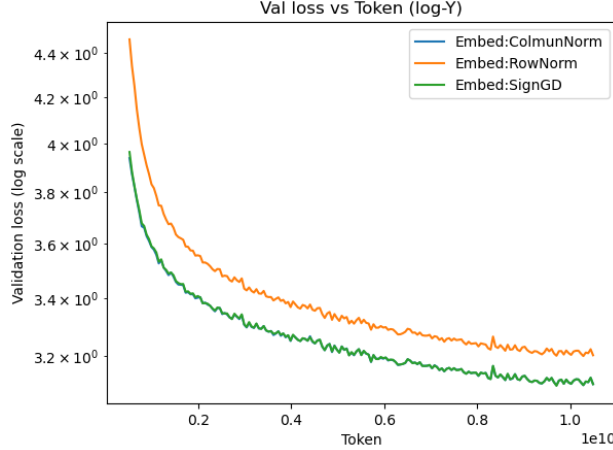


Figure 2: **Embedding layer geometry.** One-hot inputs place embedding training in the $1 \rightarrow (q, \text{mean})$ geometry, where both column normalization and SignGD are effective.

Input Word Embedding and Positional Embeddings Input word embeddings map each token to a continuous representation, while positional embeddings encode the position of each token in the sequence. The token embedding matrix has dimension $d_{\text{model}} \times \text{vocabsize}$, and the positional embedding matrix has dimension $d_{\text{model}} \times \text{contextsize}$. In both cases, the d_{in} dimension corresponds to vocabsize or contextsize, while the d_{out} dimension equals d_{model} . Importantly, the d_{in} dimensions of these embedding layers are determined by the vocabulary size or context length and therefore do not scale with the model width d_{model} . As observed by [60], this implies that for Adam-type optimizers the magnitude of parameter updates remains at an $\mathcal{O}(1)$ scale throughout training.

From an operator perspective, both token and positional embeddings act on one-hot basis vectors. Since one-hot vectors lie in the ℓ_1 unit ball, it is therefore natural to model the input space using the ℓ_1 geometry. In our framework, hidden representations are modeled in the (q, mean) geometry with $q \geq 1$, so the embedding layer can be viewed as a linear operator from ℓ_1 to the hidden-feature space, i.e., a $1 \rightarrow (q, \text{mean})$ operator. Under this operator norm,

$$\|\mathbf{W}\|_{1 \rightarrow (q, \text{mean})} = \max_c \|\mathbf{W}_{:,c}\|_{(q, \text{mean})},$$

so the geometry directly controls the scale of individual embedding vectors (the columns of the embedding matrix). This interpretation is also consistent with the structure of embedding lookups, since $\mathbf{W}\mathbf{x} = \mathbf{W}_{:,c}$ for one-hot inputs.

- (i) **SignSGD.** Our first choice models the embedding layer under the $1 \rightarrow \infty$ operator geometry. Under this geometry, the steepest-descent update reduces to applying SignSGD to the embedding parameters (Proposition 1).
- (ii) **Scaled Column Normalization.** Our second choice models the embedding layer under the $1 \rightarrow (q, \text{mean})$ operator geometry. The corresponding steepest-descent update takes the form $d_{\text{out}}^{1/q} \text{colnorm}_q(\cdot)$. The factor $d_{\text{out}}^{1/q}$ arises because the (q, mean) geometry corresponds to a rescaled ℓ_q -norm, $\|\mathbf{x}\|_{(q, \text{mean})} = n^{-1/q} \|\mathbf{x}\|_q$, for vectors in \mathbb{R}^n . Here $n = d_{\text{out}}$, since each embedding vector lies in a d_{out} -dimensional output space.

Although one-hot vectors are unit vectors in ℓ_p for any $p \geq 1$, modeling the embedding layer under the $p \rightarrow \infty$ geometry (corresponding to a $\text{rownorm}_p(\cdot)$ update) performs poorly in our experiments; see Figure 2. This observation further supports the ℓ_1 -based modeling choice for embedding inputs.

Biases and LayerNorm Parameters Bias parameters directly perturb the hidden feature representation, which lives in the (q, mean) geometry. To ensure that these updates remain safely within the feature constraint set, we adopt the ℓ_∞ geometry for all vector parameters. Since the ℓ_∞ ball is contained in the (q, mean) ball when $q \geq 1$, restricting updates to the ℓ_∞ geometry ensures that the resulting perturbation remains within the (q, mean) constraint set. Under the ℓ_∞ geometry, the steepest-descent direction is given by the sign of the gradient, leading to a SignSGD-type update without additional scaling.

LayerNorm weights \mathbf{w}^{LN} and biases \mathbf{b}^{LN} are vectors in $\mathbb{R}^{d_{\text{model}}}$. The LayerNorm weight corresponds to a diagonal linear operator acting on the hidden feature space, whose operator norm under the $(q, \text{mean}) \rightarrow (q, \text{mean})$ geometry reduces to the maximum absolute value of the diagonal entries. Consequently, the steepest-descent direction again collapses to a sign-based update. In practice, we therefore apply pure SignSGD updates to all vector parameters, including LayerNorm

weights, LayerNorm biases, and MLP biases. This scaling is consistent with the parametrization recommended by the μP theory [60].

Self-Attention In a Transformer self-attention block, the input $X \in \mathbb{R}^{\text{contextsize} \times d_{\text{model}}}$ represents the hidden features of a sequence of tokens, where contextsize denotes the sequence length and d_{model} is the model width. In the standard multi-head attention with n_{head} heads [51], each head has value dimension d_v . The input is projected into queries, keys, and values via

$$Q = XW_q, \quad K = XW_k, \quad V = XW_v,$$

where $W_q, W^k, W^v \in \mathbb{R}^{d_{\text{model}} \times (d_v n_{\text{head}})}$. The outputs from different heads are concatenated and projected back to the model dimension through the output matrix $W_o \in \mathbb{R}^{(d_v n_{\text{head}}) \times d_{\text{model}}}$. Following [51], the matrices Q, K, V are reshaped into n_{head} heads, i.e., tensors of shape $(n_{\text{head}}, \text{contextsize}, d_v)$. Each head then computes

$$\text{head}_i = \text{softmax}\left(\frac{Q_i K_i^T}{\sqrt{d_v}}\right) V_i.$$

The outputs of all heads are concatenated and projected back to the model dimension through

$$\text{MultiHead}(X) = \text{concat}(\text{head}_1, \dots, \text{head}_{n_{\text{head}}}) W_o, \quad W_o \in \mathbb{R}^{d_{\text{model}} \times (d_v n_{\text{head}})}.$$

However, in the μP parametrization [60], the authors use a normalization factor $1/d_v$, rather than $1/\sqrt{d_v}$, i.e.,

$$\text{head}_i = \text{softmax}\left(\frac{Q_i K_i^T}{d_v}\right) V_i.$$

We now provide an alternative explanation from the perspective of M -Lipschitzness and L -smoothness. To ensure that the softmax operator remains L -smooth, the magnitude of the attention logits must be controlled so that it does not grow with the network width. Under row normalization (i.e., the geometry $(p, \text{mean}) \rightarrow \ell_\infty$), both query and key vectors are bounded in the ℓ_∞ norm. Consequently, $|q^T k| \leq d_v \|q\|_\infty \|k\|_\infty = O(d_v)$, so we apply a normalization factor $1/d$ to keep the attention logits at a constant scale. In contrast, under column normalization (i.e., the geometry $(1, \text{mean}) \rightarrow (q, \text{mean})$), the query and key vectors remain bounded in the (q, mean) norm. By Lemma 5, their inner product scales as

$$q^T k = O\left(d_v^{\max\{1, \frac{2}{p}\}}\right),$$

which leads to the normalization factor $d_v^{-\max\{1, 2/p\}}$, ensuring that the attention logits remain width-independent.

Attention scaling.

- $(p, \text{mean}) \rightarrow \ell_\infty$ (row normalization): scale by $1/d_v$.
- $(1, \text{mean}) \rightarrow (q, \text{mean})$ (column normalization): scale by $d_v^{-\max\{1, 2/q\}}$.
- For Adam/SignSgd case, we recover the normalization in μP parameterization [60].

MLP A Transformer MLP block contains two weight matrices $W_1 \in \mathbb{R}^{d_{\text{fin}} \times d_{\text{model}}}$ and $W_2 \in \mathbb{R}^{d_{\text{model}} \times d_{\text{fin}}}$, where the feedforward dimension is typically $d_{\text{fin}} = 4d_{\text{model}}$. Accordingly, the d_{in} and d_{out} are $(d_{\text{model}}, d_{\text{fin}})$ for W_1 and $(d_{\text{fin}}, d_{\text{model}})$ for W_2 . Following the treatment of other bias parameters, the MLP bias is updated under the ℓ_∞ geometry, resulting in a SignSGD-type update without additional scaling.

Word Unembedding Following the μP scaling rule [60], the word *unembedding* matrix is tied to the word *embedding* matrix. Consequently, the unembedding parameters follow the same scaling as the embedding parameters, i.e., we do not scale down the learning rate for the unembedding layer.

4 Experiments

We evaluate the proposed MOGA optimizer on large-scale language model pre-training tasks and compare it against strong baselines including AdamW and Muon. Our experiments focus on three aspects: (i) learning-rate transfer across model widths, (ii) training efficiency under standard token budgets, and (iii) performance under large token budgets.

We conduct experiments on both **GPT-2** and **LLaMA** architectures. For GPT-2 models, we use the standard tokenizer with a vocabulary size 50,257 and context length 1,024, and train on the *OpenWebText* dataset [20]. For LLaMA models,

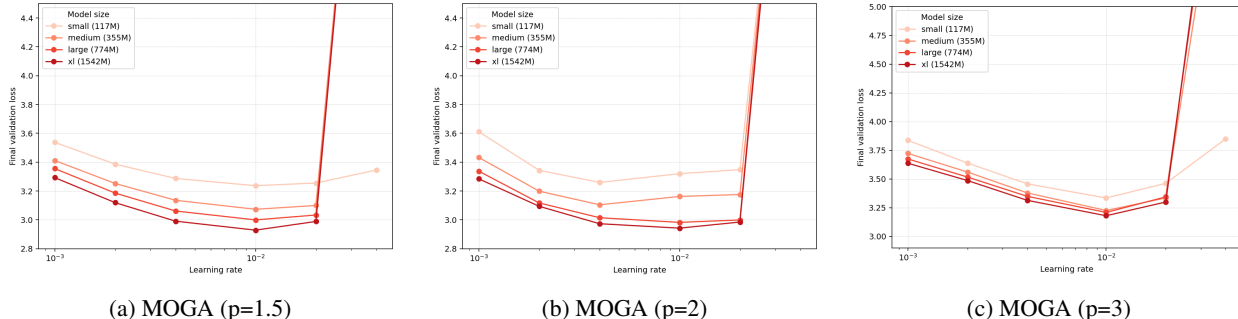


Figure 3: **Learning Rate Transfer.** Performance of MOGA from GPT-2 Small to GPT-XL. The optimal learning rate of MOGA is invariant to width.

we use vocabulary size 32,000 and context length 256, and pretrain from scratch on the *C4* dataset [42]. All experiments are conducted on four NVIDIA H100 GPUs.

We evaluate MOGA instantiated with row normalization, and compare against AdamW and Muon. The implementation code is publicly available at <https://github.com/ruihanxx/rownorm>.

4.1 Learning Rate Transfer

In this subsection, we study whether the optimal learning rate remains invariant across model widths. Details are as follows:

- *Models.* We experiment on GPT-2 models ranging from Small to XL, with hidden dimensions from 768 to 1600 and parameter counts from 124M to 1.5B. To evaluate width invariance, we instantiate MOGA with row normalization using norm parameters $p \in \{1.5, 2, 3\}$.
- *LR schedulers and training configuration.* Models are pretrained from scratch with a 3B-token budget. Due to a limited token budget, we adopt the LR schedule consisting of a linear warm-up over 10% of the training steps followed by cosine decay. The learning rate increases linearly from zero to the peak value lr_max , after which it follows a cosine annealing schedule down to the terminal learning rate $lr_min = lr_max/10$.
- *Training configurations.* The total batch size corresponds to $1024 \times 512 = 524,288$ tokens per step. We sweep the peak learning rate lr_max over $\{1 \times 10^{-3}, 2 \times 10^{-3}, 4 \times 10^{-3}, 1 \times 10^{-2}, 2 \times 10^{-2}, 4 \times 10^{-2}\}$.

As shown in Figure 3, models with substantially different parameter counts achieve their best training performance at nearly the same peak learning rate lr_max . This indicates that the optimal learning rate is effectively invariant to model width under the proposed optimizer. As a consequence, learning rates tuned on a small model can be directly transferred to larger models without additional hyperparameter search, significantly reducing the cost of scaling experiments.

This invariance holds consistently across multiple norm choices p in the row-normalization family, supporting our theoretical prediction of width-independent smoothness under the mean-normalized operator geometry. Notably, the case $p = 3$ does not satisfy the spectral assumptions typically required by μP scaling theory, yet still exhibits reliable learning-rate transfer in practice. This provides empirical evidence that our framework applies to a broader class of optimizers beyond those covered by existing μP analyses.

4.2 Standard Token Budget Experiment

For standard token budget pretraining, we experiment on **GPT-2 small** model and **LLaMA-130M** model, using approximately $\sim 1\times$ the Chinchilla-optimal number of training tokens [23]. Details are as follows:

- *LR schedulers.* We adopt the same learning-rate schedule as in Section 4.1, namely a linear warm-up over 10% of the total training steps followed by cosine decay.
- *Training configurations.* For GPT-2, we use a total batch size of 1024 with a maximum sequence length 512, corresponding to $1024 \times 512 = 524,288$ tokens per step, which is consistent with the widely adopted configuration [41] for GPT-2 small training. For LLaMA-130M, we follow [54] and use a total batch size of 512 with a maximum sequence length 256, yielding $512 \times 256 = 131,072$ tokens per step.

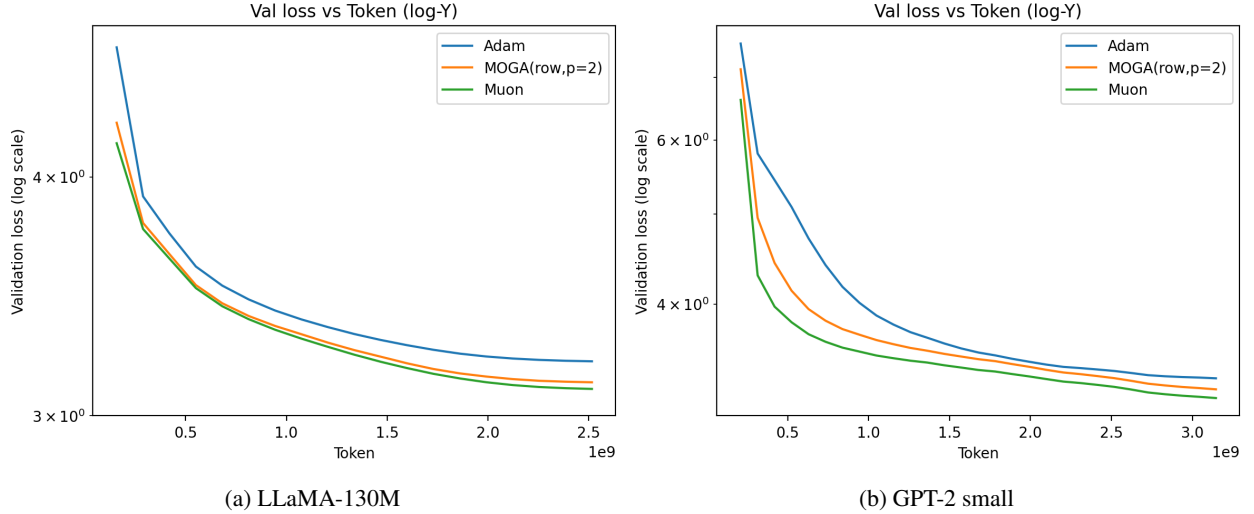


Figure 4: **Standard Token Budget Experiment.** Performance of MOGA on GPT-2 small model and LLaMA-130M model compared to Muon and AdamW with $1\times$ chinchilla optimal token budget.

- *Hyperparameters.* For the GPT-2 models, AdamW uses $\beta_1 = 0.9$, $\beta_2 = 0.95$, and weight decay $\lambda = 0.1$, while Muon follows the configuration of [32] with $\beta_1 = 0.95$, $\beta_2 = 0$ and weight decay $\lambda = 0.1$. For the LLaMA models, AdamW uses $\beta_1 = 0.9$, $\beta_2 = 0.999$, and weight decay $\lambda = 0$, and Muon uses $\beta_1 = 0.95$, $\beta_2 = 0$ with weight decay $\lambda = 0$. For each optimizer, the peak learning rate lr_max is tuned via a logarithmic sweep during the first training epoch. Specifically, for GPT-2 we search over $lr_max \in [8 \times 10^{-5}, 8 \times 10^{-4}]$ for AdamW, and $lr_max \in [4 \times 10^{-4}, 4 \times 10^{-3}]$ for Muon, and $lr_max \in [4 \times 10^{-3}, 4 \times 10^{-2}]$ for MOGA instantiated with row normalization using $p = 2$. For LLaMA we search over $lr_max \in [4 \times 10^{-5}, 4 \times 10^{-4}]$ for AdamW, $lr_max \in [4 \times 10^{-4}, 4 \times 10^{-3}]$ for Muon, and $lr_max \in [4 \times 10^{-3}, 4 \times 10^{-2}]$ for MOGA instantiated with row normalization using $p = 2$. All models are subsequently trained using the optimizer-specific lr_max that achieves the best validation performance.

As shown in Figure 4, on the LLaMA-130M model, MOGA achieves performance comparable to Muon, with both optimizers converging substantially faster than AdamW. On the GPT-2 small model, the convergence behavior of MOGA lies between that of Muon and AdamW, demonstrating competitive optimization efficiency across architectures.

4.3 Large Token Budget Experiment

We evaluate optimization performance under a large-token regime, using approximately $\sim 8\times$ the Chinchilla-optimal number of training tokens. Experiments are conducted on **GPT-2 Small** and **LLaMA-130M** models. Details are follows:

- *LR schedulers.* We follow the same schedule as in Section 4.1, but with different warm-up ratios. For both GPT-2 Small and LLaMA-130M, we use a linear warm-up over 2.5% of the total steps followed by cosine decay.
- *Training configurations.* We use the same training setup as in Section 4.2.
- *Hyperparameters.* The hyperparameter settings are the same as those in Section 4.2, except for the learning-rate search ranges specified below. For GPT-2 we search over $lr_max \in [8 \times 10^{-5}, 8 \times 10^{-4}]$ for AdamW and $lr_max \in [4 \times 10^{-4}, 4 \times 10^{-3}]$ for Muon. For LLaMA we search over $lr_max \in [4 \times 10^{-5}, 4 \times 10^{-4}]$ for AdamW, $lr_max \in [4 \times 10^{-4}, 4 \times 10^{-3}]$ for Muon, and $lr_max \in [4 \times 10^{-3}, 4 \times 10^{-2}]$ for MOGA instantiated with row normalization using $p = 2$.

As shown in Figure 5, the MOGA optimizer exhibits a clear speed advantage in the later stages of training, particularly in the low-loss regime. In the GPT-2 Small experiment, MOGA performs comparably to Muon and consistently outperforms AdamW. Notably, the loss curve of MOGA shows a steeper downward trend toward the end of training, suggesting that with a longer training horizon it would likely surpass Muon. In the LLaMA-130 experiments, MOGA already achieves the best overall performance among all optimizers. These results indicate that MOGA is particularly

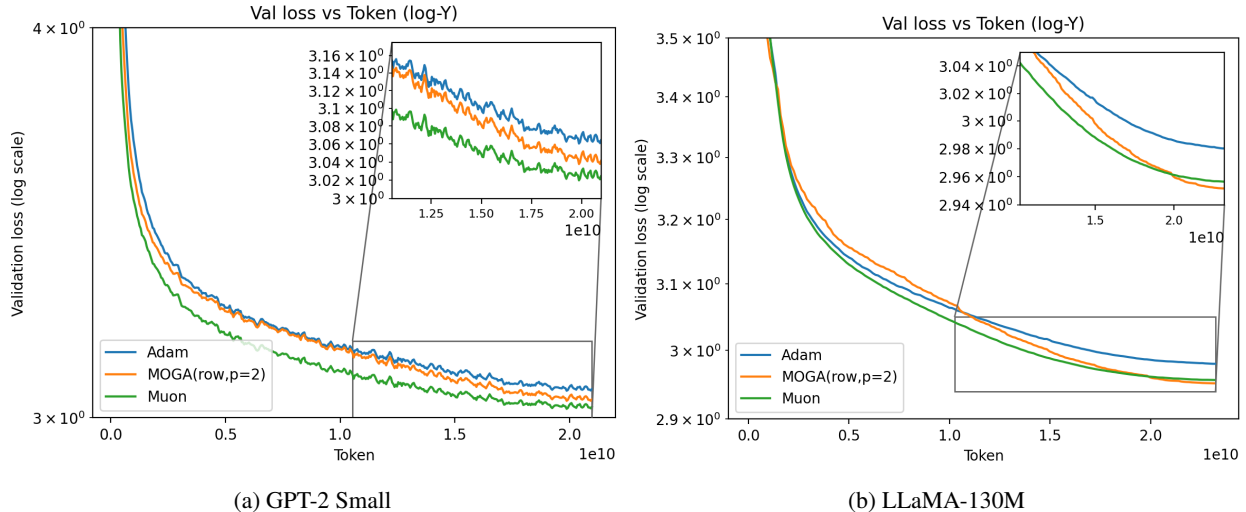


Figure 5: **Large Token Budget Experiment.** Performance of MOGA on GPT-2 small model and LLaMA-130M model compared to Muon and AdamW. MOGA exhibits a faster convergence speed in the low-loss stage.

advantageous for longer training runs and in the low-loss regime, which is highly valuable in practical large-scale training.

5 Discussion

5.1 Related Work

Optimizers for Modern Language Models. Modern large-scale neural networks and language models commonly rely on variants of adaptive gradient methods, beginning with AdaGrad [15, 57]. Most practical optimizers employ diagonal preconditioning, as in Adam [26, 43, 33], or block-wise approximations such as Adafactor [47], LAMB [62], and Adam-Mini [63]. More expressive preconditioning strategies have also been explored. For example, Shampoo [21] and SOAP [53] use structured tensor-based preconditioners to approximate curvature information. Another line of work views second-order methods as the gold standard for neural network optimization. In particular, natural-gradient approaches approximate the Fisher information matrix [38, 44, 40], while recent works such as [30, 53] develop scalable approximations inspired by SOAP-style preconditioning. More recently, [58, 1] proposed ASGO (One-Sided Shampoo), which applies a one-sided variant of the Shampoo preconditioner.

Gradient Normalization. Starting from SignSGD [7], a line of work has connected gradient normalization with steepest descent under alternative norms. For example, Muon [24] formulates neural network optimization as steepest descent under the spectral norm, which leads to whitening the gradient matrix. Similarly, [19] study steepest descent under the $\ell_1 \rightarrow \ell_2$ operator norm, which results in column normalization of the gradient. Several recent works employ row-wise or doubly normalized updates. In particular, [34] combine row normalization with the matrix sign function to normalize the gradient, while [46] use the Sinkhorn algorithm to normalize the gradient simultaneously across rows and columns. In contrast, our framework considers the $(2, \text{mean}) \rightarrow \ell_\infty$ geometry, which requires an additional scaling factor of $1/\sqrt{d_{\text{in}}}$ in the update. Normalization-based methods have recently attracted attention because they exhibit favorable theoretical properties in challenging regimes. For instance, they can achieve improved guarantees under heavy-tailed noise [56, 16] and for ill-conditioned optimization problems [35]. Their convergence properties under various L -smoothness assumptions have also been studied in [29, 39, 48, 19, 45, 27, 13, 52]. Our work takes a different perspective. Rather than analyzing specific normalization schemes, we study when a neural network objective satisfies an L -smoothness condition and use this criterion to determine which normalization geometry is appropriate. The closest related work is [14], which studies when spectral descent outperforms Euclidean gradient descent by characterizing the nuclear rank of the gradient and estimating this quantity in a random feature model. Another related line of work is [49], which proposes an isotropic curvature model to analyze spectral normalization and derives optimal updates using second-order information. It would be interesting to combine such curvature models with alternative geometries to design new normalization-based algorithms; we leave this direction for future work.

Hyperparameter Transfer. Hyperparameter transfer, particularly learning-rate transfer, aims to reuse a learning rate (or schedule) tuned on a small network when training a larger one, thereby avoiding per-run hyperparameter search. The goal is to identify simple scaling rules that preserve stability and performance under changes in width, depth, batch size, and optimizer details. A prominent line of work is based on Tensor Programs. [59, 60] analyze the infinite-width limit of forward and backward dynamics and derive parameterizations that keep activation and gradient scales consistent across widths. This framework yields concrete rules for transferring learning rates from small networks to larger ones with minimal retuning. However, the analysis is anchored in infinite-width initialization scaling and early training dynamics, and therefore does not fully capture later training effects such as finite-width corrections, evolving feature correlations, or distribution shifts. A complementary approach is proposed by [36], who upscale a trained small network to a wider one by deterministically duplicating neurons (equivalently, replicating parameter tensors with structured rescaling) so that the widened model initially computes exactly the same function. With a corresponding rescaling of optimizer hyperparameters, the widened model follows an equivalent training trajectory to the small model. Both approaches justify learning-rate transfer only for specific structured regimes (e.g., random initialization or deterministically upscaled networks). In contrast, our worst-case analysis establishes a width-independent M -Lipschitz and L -smoothness bounds, providing a principled guarantee for learning-rate transfer beyond these specialized constructions.

5.2 How to select p and q ?

In Theorem 2, both the M -Lipschitz and L -smoothness bounds are derived under the assumption that the network parameters lie in a width-independent bounded set under the chosen geometry. In particular, the analysis is carried out on a compact set Ω_c . Such geometric constraints inevitably restrict the function class represented by the network. In this subsection, we examine these constraints from the perspective of approximation capacity and use them to guide the choice of geometry.

To understand the implication of this assumption, we view the compact set Ω_c as inducing a hypothesis class through the network output map. For each parameter tuple $(\mathbf{W}_{1:\ell}, \mathbf{b}_{1:\ell}) \in \Omega_c$, the network produces an output $y_\ell(\mathbf{x})$, and hence defines a predictor. Therefore, the constraint Ω_c implicitly determines a function class \mathcal{F}_{Ω_c} , and different choices of geometry lead to different hypothesis classes.

We recall the standard decomposition of the expected risk in supervised learning. Let h^* denote the target function and $\hat{h}_{\mathcal{F}}$ the model learned by an algorithm. The excess risk is defined as

$$\mathcal{R} := \mathbb{E}_{\mathbb{P}}[\mathcal{L}(\hat{h}_{\mathcal{F}}(\mathbf{x}))] - \mathbb{E}_{\mathbb{P}}[\mathcal{L}(h^*(\mathbf{x}))].$$

It can be decomposed as

$$\begin{aligned} \mathcal{R} \leq & \underbrace{\inf_{h \in \mathcal{F}} \mathbb{E}_{\mathbb{P}}[\mathcal{L}(h(\mathbf{x}))] - \mathbb{E}_{\mathbb{P}}[\mathcal{L}(h^*(\mathbf{x}))]}_{\text{approximation error}} + \underbrace{\mathbb{E}_{\mathbb{P}_n}[\mathcal{L}(\hat{h}_{\mathcal{F}}(\mathbf{x}))] - \mathbb{E}_{\mathbb{P}}[\mathcal{L}(h^*(\mathbf{x}))]}_{\text{optimization error}} \\ & + 2 \underbrace{\sup_{h \in \mathcal{F}} |\mathbb{E}_{\mathbb{P}_n}[\mathcal{L}(h(\mathbf{x}))] - \mathbb{E}_{\mathbb{P}}[\mathcal{L}(h(\mathbf{x}))]|}_{\text{generalization error}}. \end{aligned} \quad (13)$$

Here $\mathbb{E}_{\mathbb{P}}[\cdot]$ denotes expectation with respect to the true (unknown) data distribution \mathbb{P} , while $\mathbb{E}_{\mathbb{P}_n}[\cdot]$ denotes the empirical expectation over n samples. The function class \mathcal{F} represents the hypothesis space, $h^*_{\mathcal{F}} = \arg \min_{h \in \mathcal{F}} \mathbb{E}_{\mathbb{P}}[\mathcal{L}(h(\mathbf{x}))]$ denotes the best approximation of h^* inside \mathcal{F} , and $\hat{h}_{\mathcal{F}} = \arg \min_{h \in \mathcal{F}} \mathbb{E}_{\mathbb{P}_n}[\mathcal{L}(h(\mathbf{x}))]$ denotes the empirical risk minimizer. In this decomposition, the approximation error quantifies the expressiveness of the hypothesis class \mathcal{F} , the optimization error measures the suboptimality of the learning algorithm, and the generalization error captures the gap between training performance and unseen data.

The choice of norm influences all three components of the risk decomposition. It determines the geometry of the hypothesis space and thus its approximation power, affects gradients, conditioning, and convergence in optimization, and regulates the effective capacity of the model in generalization. We now formalize the notion of a stronger norm.

Definition 4 (Stronger norm). *Let $\|\cdot\|_A$ and $\|\cdot\|_B$ be two norms. We say that $\|\cdot\|_A$ is stronger than $\|\cdot\|_B$ if*

$$\{\mathbf{X} : \|\mathbf{X}\|_A \leq 1\} \subseteq \{\mathbf{X} : \|\mathbf{X}\|_B \leq 1\}.$$

In other words, a stronger norm induces a smaller unit ball in the parameter space. This geometric relationship underlies the trade-offs between optimization, approximation, and generalization discussed below.

- (i) **Optimization:** Since stronger norms induce smaller unit balls in the parameter space, the M -Lipschitz and L -smoothness constants of the objective typically decrease when measured under the stronger geometry. Consequently, gradient-based methods can adopt larger learning rates while maintaining stability, which leads to faster convergence.

- (ii) **Approximation:** Norm constraints restrict the feasible parameter set and therefore determine the hypothesis class that the network can represent. If $\|\cdot\|_A$ is stronger than $\|\cdot\|_B$, then the feasible set under $\|\cdot\|_A$ is smaller, which induces a more restricted hypothesis class. As a result, stronger norms may reduce the approximation capacity of the network.
- (iii) **Generalization:** Norm constraints also regulate the effective capacity of the model. By limiting the magnitude of weights, stronger norms prevent the network from fitting overly complex or noisy patterns in the training data, which often improves generalization performance.

Overall, norm selection introduces an intrinsic trade-off. Stronger norms improve optimization and generalization through tighter control of the parameter space, but may reduce approximation capacity, whereas weaker norms enlarge the hypothesis class at the potential cost of worse smoothness and generalization behavior. We now examine the behavior of several normalization schemes under this approximation–optimization trade-off. While the unit balls of different operator norms are not directly comparable due to dimension-dependent norm equivalence, the scaling behavior still provides a useful proxy for how restrictive each geometry becomes as the network width grows:

- **Muon under (2, mean) \rightarrow (2, mean) Geometry.** Under this geometry, the L -smoothness constant scales as $\mathcal{O}(\sqrt{w})$, indicating that the optimization landscape becomes increasingly rough as the network widens. However, the admissible scale of the weight matrix remains $\mathcal{O}(1)$ because the RMS normalization rescales the weights by the matrix dimension. As a result, the feasible parameter set does not shrink with width, and the representational capacity of the network remains stable.
- **Column normalization under (1, mean) \rightarrow (q , mean) Geometry.** This geometry achieves width-independent smoothness when $q \geq 2$, leading to a well-conditioned optimization landscape. However, the constraint induced by the operator norm becomes increasingly restrictive as the width grows. To see this, note that under the (1, mean) geometry the input norm scales as $\mathcal{O}(w^{-1})$, while the (q , mean) output norm scales as $\mathcal{O}(w^{-1/q})$. Since the operator norm measures the maximum amplification ratio between output and input norms, maintaining a bounded operator norm requires the weight magnitudes to shrink by a factor $\mathcal{O}(w^{-(q-1)/q})$. Consequently, the admissible scale of weight columns decreases as $\mathcal{O}(w^{-(q-1)/q})$, which shrinks rapidly with width. Thus, although optimization becomes easier, the representational capacity of the network is significantly constrained.
- **Row normalization under (p , mean) \rightarrow ∞ Geometry.** Under this geometry, the (p , mean) input norm scales as $\mathcal{O}(w^{-1/p})$, while the ℓ_∞ output norm remains $\mathcal{O}(1)$. Maintaining a bounded operator norm therefore requires the weight magnitudes to shrink at a rate $\mathcal{O}(w^{-1/p})$. Compared with column normalization, whose admissible scale shrinks as $\mathcal{O}(w^{-(q-1)/q})$, row normalization contracts the feasible parameter set much more slowly. In particular, when $p, q \geq 2$ we have

$$\frac{1}{p} \leq \frac{1}{2} < \frac{q-1}{q},$$

so the constraint imposed by row normalization becomes less restrictive with width compared to column normalization. Consequently, this scaling behavior suggests that row normalization may retain a richer hypothesis class while still benefiting from improved smoothness.

Message: Stronger norms impose tighter constraints on the parameter space, which improves smoothness of the optimization landscape but restricts the expressive capacity of the model. Norm selection therefore introduces an optimization–approximation trade-off.

	Row Normalization	Column Normalization	Muon
Norm	$\ \cdot\ _{(p,\text{mean}) \rightarrow \ell_\infty}$	$\ \cdot\ _{(1,\text{mean}) \rightarrow (q,\text{mean})}$	$\ \cdot\ _{(2,\text{mean}) \rightarrow (2,\text{mean})}$
L -smoothness	$\mathcal{O}(1)$	$\mathcal{O}(1)$ ($q \geq 2$)	$\mathcal{O}(\sqrt{w})$
Weight scaling	$\mathcal{O}(w^{-1/p})$	$\mathcal{O}(w^{-(q-1)/q})$	$\mathcal{O}(1)$

For $p, q \geq 2$, both row and column normalization achieve width-independent smoothness. Since $\frac{1}{p} < \frac{q-1}{q}$, the admissible weight scale under row normalization shrinks more slowly with width than under column normalization, suggesting a better balance between smooth optimization and representational flexibility.

6 Conclusion

In this paper, we study the width-scaling behavior of neural optimizers through the lens of matrix-operator-norm steepest descent, aiming to understand how optimization geometry determines scalable learning-rate rules. We show that many popular optimizers, including AdamW, Muon, Lion, and row/column normalization methods, can be unified as instances

of steepest descent under different matrix operator norms. However, neural networks are not dimension-independently Lipschitz under arbitrary matrix operator norms. In particular, classical $p \rightarrow q$ operator norms fail to propagate stability across layers: Their Lipschitz bounds do not compose cleanly, leading to width-dependent distortions in the overall Lipschitz constant and unstable learning-rate scaling.

To address this issue, we introduce the *mean normalized operator norm* $(p, \text{mean}) \rightarrow (q, \text{mean})$ with $p \leq q$, which rescales the geometry to match network width. Under this geometry, operator norms compose stably across layers, making the network forward map M -Lipschitz with no width dependence. We further analyze gradient sensitivity and prove that the objective becomes L -smooth with width-independent optimal learning rates. Our theory identifies two width-stable geometries:

$$(1, \text{mean}) \rightarrow (q, \text{mean}) \quad (q \geq 2), \quad (p, \text{mean}) \rightarrow \infty,$$

and shows that the latter preserves a less restrictive parameter scaling, yielding a more favorable optimization–approximation trade-off. This observation motivates a new optimizer, *rescaled row-normalized steepest descent*, which applies a power transform followed by per-row normalization.

Based on our theory, we propose MOGA (Matrix Operator Geometry Aware), a width-aware optimizer that requires only row/column-wise normalization and enables reliable learning-rate transfer across model widths, allowing models of substantially different sizes to share nearly the same peak learning rate without extensive retuning. Large-scale pre-training experiments on GPT-2 and LLaMA further show that MOGA is competitive with Muon and can be substantially faster in large-token and low-loss regimes, where optimization stability is most critical. Overall, our results yield a L -smoothness based geometry-aware principle for constructing neural optimizers that remain stable under width scaling and preserve consistent learning dynamics as model size grows.

Acknowledgement We thank Jose Blanchet, Fanghui Liu, Jianhao Ma, Jorge Nocedal, Weijie Su, Kaiyue Wen, Lei Wu, Tengyuan Liang, Yinuo Ren, Yinyu Ye, Lexing Ying and Jiacheng You for their valuable feedback.

References

- [1] K. An, Y. Liu, R. Pan, Y. Ren, S. Ma, D. Goldfarb, and T. Zhang. Asgo: Adaptive structured gradient optimization. *arXiv preprint arXiv:2503.20762*, 2025.
- [2] Y. Bahri, E. Dyer, J. Kaplan, J. Lee, and U. Sharma. Explaining neural scaling laws. *Proceedings of the National Academy of Sciences*, 121(27):e2311878121, 2024.
- [3] L. Balles and P. Hennig. Dissecting adam: The sign, magnitude and variance of stochastic gradients. In *International Conference on Machine Learning*, pages 404–413. PMLR, 2018.
- [4] J. Bernstein and L. Newhouse. Modular duality in deep learning. *arXiv preprint arXiv:2410.21265*, 2024.
- [5] J. Bernstein and L. Newhouse. Old optimizer, new norm: An anthology. *arXiv preprint arXiv:2409.20325*, 2024.
- [6] J. Bernstein, A. Vahdat, Y. Yue, and M.-Y. Liu. On the distance between two neural networks and the stability of learning. *Advances in Neural Information Processing Systems*, 33:21370–21381, 2020.
- [7] J. Bernstein, Y.-X. Wang, K. Azizzadenesheli, and A. Anandkumar. signsgd: Compressed optimisation for non-convex problems. In *International conference on machine learning*, pages 560–569. PMLR, 2018.
- [8] D. E. Carlson, E. Collins, Y.-P. Hsieh, L. Carin, and V. Cevher. Preconditioned spectral descent for deep learning. *Advances in neural information processing systems*, 28, 2015.
- [9] L. Chen, J. Li, and Q. Liu. Muon optimizes under spectral norm constraints. *arXiv preprint arXiv:2506.15054*, 2025.
- [10] L. Chen, B. Liu, K. Liang, and Q. Liu. Lion secretly solves constrained optimization: As lyapunov predicts. *arXiv preprint arXiv:2310.05898*, 2023.
- [11] X. Chen, C. Liang, D. Huang, E. Real, K. Wang, H. Pham, X. Dong, T. Luong, C.-J. Hsieh, Y. Lu, et al. Symbolic discovery of optimization algorithms. *Advances in neural information processing systems*, 36:49205–49233, 2023.
- [12] C. Cortes, L. D. Jackel, S. Solla, V. Vapnik, and J. Denker. Learning curves: Asymptotic values and rate of convergence. *Advances in neural information processing systems*, 6, 1993.
- [13] M. Crawshaw, C. Modi, M. Liu, and R. M. Gower. An exploration of non-euclidean gradient descent: Muon and its many variants. *arXiv preprint arXiv:2510.09827*, 2025.
- [14] D. Davis and D. Drusvyatskiy. When do spectral gradient updates help in deep learning? *arXiv preprint arXiv:2512.04299*, 2025.
- [15] J. Duchi, E. Hazan, and Y. Singer. Adaptive subgradient methods for online learning and stochastic optimization. *Journal of machine learning research*, 12(7), 2011.
- [16] Y. Fang, J. Demmel, and J. Lavaei. Why is normalization preferred? a worst-case complexity theory for stochastically preconditioned sgd under heavy-tailed noise, 2026.
- [17] T. Flynn. The duality structure gradient descent algorithm: analysis and applications to neural networks. *arXiv preprint arXiv:1708.00523*, 2017.

- [18] N. Ghosh, D. Wu, and A. Bietti. Understanding the mechanisms of fast hyperparameter transfer. *arXiv preprint arXiv:2512.22768*, 2025.
- [19] A. Glentis, J. Li, A. Han, and M. Hong. A minimalist optimizer design for llm pretraining. *arXiv preprint arXiv:2506.16659*, 2025.
- [20] A. Gokaslan, V. Cohen, E. Pavlick, and S. Tellex. Openwebtext corpus. <http://Skyllion007.github.io/OpenWebTextCorpus>, 2019.
- [21] V. Gupta, T. Koren, and Y. Singer. Shampoo: Preconditioned stochastic tensor optimization. In *International Conference on Machine Learning*, pages 1842–1850. PMLR, 2018.
- [22] J. Hestness, S. Narang, N. Ardalani, G. Diamos, H. Jun, H. Kianinejad, M. M. A. Patwary, Y. Yang, and Y. Zhou. Deep learning scaling is predictable, empirically. *arXiv preprint arXiv:1712.00409*, 2017.
- [23] J. Hoffmann, S. Borgeaud, A. Mensch, E. Buchatskaya, T. Cai, E. Rutherford, D. d. L. Casas, L. A. Hendricks, J. Welbl, A. Clark, et al. Training compute-optimal large language models. *arXiv preprint arXiv:2203.15556*, 2022.
- [24] K. Jordan, Y. Jin, V. Boza, J. You, F. Cesista, L. Newhouse, and J. Bernstein. Muon: An optimizer for hidden layers in neural networks. *Cited on*, page 10, 2024.
- [25] J. Kaplan, S. McCandlish, T. Henighan, T. B. Brown, B. Chess, R. Child, S. Gray, A. Radford, J. Wu, and D. Amodei. Scaling laws for neural language models. *arXiv preprint arXiv:2001.08361*, 2020.
- [26] D. P. Kingma and J. Ba. Adam: A method for stochastic optimization. *arXiv preprint arXiv:1412.6980*, 2014.
- [27] D. Kovalev. Understanding gradient orthogonalization for deep learning via non-euclidean trust-region optimization. *arXiv preprint arXiv:2503.12645*, 2025.
- [28] T. Large, Y. Liu, M. Huh, H. Bahng, P. Isola, and J. Bernstein. Scalable optimization in the modular norm. *Advances in Neural Information Processing Systems*, 37:73501–73548, 2024.
- [29] J. Li and M. Hong. A note on the convergence of muon. *arXiv preprint arXiv:2502.02900*, 2025.
- [30] W. Lin, F. Dangel, R. Eschenhagen, J. Bae, R. E. Turner, and A. Makhzani. Can we remove the square-root in adaptive gradient methods? a second-order perspective. *arXiv preprint arXiv:2402.03496*, 2024.
- [31] J. Liu, J. Su, X. Yao, Z. Jiang, G. Lai, Y. Du, Y. Qin, W. Xu, E. Lu, J. Yan, et al. Muon is scalable for llm training. *arXiv preprint arXiv:2502.16982*, 2025.
- [32] Y. Liu, A. Yuan, and Q. Gu. Mars-m: When variance reduction meets matrices. *arXiv preprint arXiv:2510.21800*, 2025.
- [33] I. Loshchilov and F. Hutter. Decoupled weight decay regularization. *arXiv preprint arXiv:1711.05101*, 2017.
- [34] C. Ma, W. Gong, M. Scetbon, and E. Meeds. Swan: Sgd with normalization and whitening enables stateless llm training. *arXiv preprint arXiv:2412.13148*, 2024.
- [35] J. Ma, Y. Huang, Y. Chi, and Y. Chen. Preconditioning benefits of spectral orthogonalization in muon. *arXiv preprint arXiv:2601.13474*, 2026.
- [36] Y. Ma, N. Chen, M. D’iaz, S. Hayou, D. Kunisky, and S. Villar. up scaling small models: Principled warm starts and hyperparameter transfer. *arXiv preprint arXiv:2602.10545*, 2026.
- [37] C. J. Maddison, D. Paulin, Y. W. Teh, and A. Doucet. Dual space preconditioning for gradient descent. *SIAM Journal on Optimization*, 31(1):991–1016, 2021.
- [38] J. Martens and R. Grosse. Optimizing neural networks with kronecker-factored approximate curvature. In *International conference on machine learning*, pages 2408–2417. PMLR, 2015.
- [39] T. Pethick, W. Xie, K. Antonakopoulos, Z. Zhu, A. Silveti-Falls, and V. Cevher. Training deep learning models with norm-constrained lmos. *arXiv preprint arXiv:2502.07529*, 2025.
- [40] O. Pooladzandi and X.-L. Li. Curvature-informed sgd via general purpose lie-group preconditioners. *arXiv preprint arXiv:2402.04553*, 2024.
- [41] A. Radford, J. Wu, R. Child, D. Luan, D. Amodei, I. Sutskever, et al. Language models are unsupervised multitask learners. *OpenAI blog*, 1(8):9, 2019.
- [42] C. Raffel, N. Shazeer, A. Roberts, K. Lee, S. Narang, M. Matena, Y. Zhou, W. Li, and P. J. Liu. Exploring the limits of transfer learning with a unified text-to-text transformer. *Journal of machine learning research*, 21(140):1–67, 2020.
- [43] S. J. Reddi, S. Kale, and S. Kumar. On the convergence of adam and beyond. *arXiv preprint arXiv:1904.09237*, 2019.
- [44] Y. Ren and D. Goldfarb. Tensor normal training for deep learning models. *Advances in Neural Information Processing Systems*, 34:26040–26052, 2021.
- [45] A. Riabinin, E. Shulgin, K. Gruntkowska, and P. Richtárik. Gluon: Making muon & scion great again!(bridging theory and practice of lmo-based optimizers for llms). *arXiv preprint arXiv:2505.13416*, 2025.
- [46] M. Scetbon, C. Ma, W. Gong, and E. Meeds. Gradient multi-normalization for stateless and scalable llm training. *arXiv preprint arXiv:2502.06742*, 2025.
- [47] N. Shazeer and M. Stern. Adafactor: Adaptive learning rates with sublinear memory cost. In *International Conference on Machine Learning*, pages 4596–4604. PMLR, 2018.
- [48] W. Shen, R. Huang, M. Huang, C. Shen, and J. Zhang. On the convergence analysis of muon. *arXiv preprint arXiv:2505.23737*, 2025.

- [49] W. Su. Isotropic curvature model for understanding deep learning optimization: Is gradient orthogonalization optimal?, 2025.
- [50] M. Tuddenham, A. Prügel-Bennett, and J. Hare. Orthogonalising gradients to speed up neural network optimisation. *arXiv preprint arXiv:2202.07052*, 2022.
- [51] A. Vaswani, N. Shazeer, N. Parmar, J. Uszkoreit, L. Jones, A. N. Gomez, Ł. Kaiser, and I. Polosukhin. Attention is all you need. *Advances in neural information processing systems*, 30, 2017.
- [52] A. Veprikov, A. Bolatov, S. Horváth, A. Beznosikov, M. Takác, and S. Hanzely. Preconditioned norms: A unified framework for steepest descent, quasi-newton and adaptive methods. *arXiv preprint arXiv:2510.10777*, 2025.
- [53] N. Vyas, D. Morwani, R. Zhao, M. Kwun, I. Shapira, D. Brandfonbrener, L. Janson, and S. Kakade. Soap: Improving and stabilizing shampoo using adam. *arXiv preprint arXiv:2409.11321*, 2024.
- [54] J. Wang, P. Zhou, Y. Dong, H. Li, J. Li, X. Zhou, Q. Lao, C. Fang, and Z. Lin. Conda: Column-normalized adam for training large language models faster. *arXiv preprint arXiv:2509.24218*, 2025.
- [55] M. Wang, J. Wang, J. Zhang, W. Wang, P. Pei, X. Cai, L. Wu, et al. Gradpower: Powering gradients for faster language model pre-training. *arXiv preprint arXiv:2505.24275*, 2025.
- [56] S. Wang, F. Zhang, J. Li, C. Du, C. Du, T. Pang, Z. Yang, M. Hong, and V. Y. Tan. Muon outperforms adam in tail-end associative memory learning. *arXiv preprint arXiv:2509.26030*, 2025.
- [57] R. Ward, X. Wu, and L. Bottou. Adagrad stepsizes: Sharp convergence over nonconvex landscapes. *Journal of Machine Learning Research*, 21(219):1–30, 2020.
- [58] S. Xie, T. Wang, S. Reddi, S. Kumar, and Z. Li. Structured preconditioners in adaptive optimization: A unified analysis. *arXiv preprint arXiv:2503.10537*, 2025.
- [59] G. Yang and E. J. Hu. Tensor programs iv: Feature learning in infinite-width neural networks. In *International Conference on Machine Learning*, pages 11727–11737. PMLR, 2021.
- [60] G. Yang, E. J. Hu, I. Babuschkin, S. Sidor, X. Liu, D. Farhi, N. Ryder, J. Pachocki, W. Chen, and J. Gao. Tensor programs v: Tuning large neural networks via zero-shot hyperparameter transfer. *arXiv preprint arXiv:2203.03466*, 2022.
- [61] G. Yang, J. B. Simon, and J. Bernstein. A spectral condition for feature learning. *arXiv preprint arXiv:2310.17813*, 2023.
- [62] Y. You, J. Li, S. Reddi, J. Hseu, S. Kumar, S. Bhojanapalli, X. Song, J. Demmel, K. Keutzer, and C.-J. Hsieh. Large batch optimization for deep learning: Training bert in 76 minutes. *arXiv preprint arXiv:1904.00962*, 2019.
- [63] Y. Zhang, C. Chen, Z. Li, T. Ding, C. Wu, D. P. Kingma, Y. Ye, Z.-Q. Luo, and R. Sun. Adam-mini: Use fewer learning rates to gain more. *arXiv preprint arXiv:2406.16793*, 2024.

A Some Useful Lemmas

In this appendix, we provide the missing proofs in the main context.

We begin with a standard lemma relating Lipschitz continuity to bounded directional derivatives, which was used in Theorem 1.

Lemma 1. *Let $\Omega \subset \mathbb{R}^{m \times n}$ be a convex norm ball, and let $f : \Omega \rightarrow \mathbb{R}$ be differentiable on Ω . Fix any norm $\|\cdot\|$ on $\mathbb{R}^{m \times n}$. Suppose there exists a constant $M > 0$ such that*

$$\sup_{\|\Delta \mathbf{Z}\| \leq 1} |\nabla f(\mathbf{Z})[\Delta \mathbf{Z}]| \leq M, \quad \forall \mathbf{Z} \in \Omega.$$

Then f is M -Lipschitz continuous on Ω with respect to $\|\cdot\|$, i.e.,

$$|f(\mathbf{Z}) - f(\mathbf{Z}')| \leq M \|\mathbf{Z} - \mathbf{Z}'\|, \quad \forall \mathbf{Z}, \mathbf{Z}' \in \Omega.$$

Proof. Proof of Lemma 1. Fix $\mathbf{Z}, \mathbf{Z}' \in \Omega$ and define the line segment $\mathbf{Z}(t) := (1-t)\mathbf{Z}' + t\mathbf{Z} = \mathbf{Z}' + t(\mathbf{Z} - \mathbf{Z}')$, $t \in [0, 1]$. Since Ω is a norm ball, it is convex, and hence $\mathbf{Z}(t) \in \Omega$ for all $t \in [0, 1]$. By the fundamental theorem of calculus applied along the line segment, we have

$$f(\mathbf{Z}) - f(\mathbf{Z}') = \int_0^1 \nabla f(\mathbf{Z}(t))[\mathbf{Z} - \mathbf{Z}'] dt.$$

If $\mathbf{Z} = \mathbf{Z}'$, the claim is trivial. Otherwise let $\Delta \mathbf{Z} := \frac{\mathbf{Z} - \mathbf{Z}'}{\|\mathbf{Z} - \mathbf{Z}'\|}$, so that $\|\Delta \mathbf{Z}\| = 1$. Then, for all $t \in [0, 1]$, the assumed bound implies

$$|\nabla f(\mathbf{Z}(t))[\mathbf{Z} - \mathbf{Z}']| = \|\mathbf{Z} - \mathbf{Z}'\| |\nabla f(\mathbf{Z}(t))[\Delta \mathbf{Z}]| \leq M \|\mathbf{Z} - \mathbf{Z}'\|.$$

Therefore,

$$|f(\mathbf{Z}) - f(\mathbf{Z}')| \leq \int_0^1 M \|\mathbf{Z} - \mathbf{Z}'\| dt = M \|\mathbf{Z} - \mathbf{Z}'\|.$$

This proves that f is M -Lipschitz continuous on Ω with respect to $\|\cdot\|$. \square

Lemma 2. Let $\Omega \subset \mathbb{R}^{m \times n}$ be a convex set, and let $f : \Omega \rightarrow \mathbb{R}$ be twice differentiable on Ω . Fix any norm $\|\cdot\|$ on $\mathbb{R}^{m \times n}$, and let $\|\cdot\|_*$ denote its dual norm. Suppose there exists $L > 0$ such that

$$\sup_{\|\Delta \mathbf{Z}^1\| \leq 1, \|\Delta \mathbf{Z}^2\| \leq 1} |\nabla^2 f(\mathbf{Z})[\Delta \mathbf{Z}^1, \Delta \mathbf{Z}^2]| \leq L, \quad \forall \mathbf{Z} \in \Omega.$$

Then f is L -smooth on Ω with respect to $\|\cdot\|$, i.e.,

$$\|\nabla f(\mathbf{Z}) - \nabla f(\mathbf{Z}')\|_* \leq L \|\mathbf{Z} - \mathbf{Z}'\|, \quad \forall \mathbf{Z}, \mathbf{Z}' \in \Omega.$$

Proof. Proof of Lemma 2. Fix $\mathbf{Z}, \mathbf{Z}' \in \Omega$ and define the line segment $\mathbf{Z}(t) := \mathbf{Z}' + t(\mathbf{Z} - \mathbf{Z}')$ for $t \in [0, 1]$. Since Ω is convex, $\mathbf{Z}(t) \in \Omega$ for all $t \in [0, 1]$. For any direction $\Delta \mathbf{Z}^1$, the fundamental theorem of calculus applied along the segment yields

$$\nabla f(\mathbf{Z})[\Delta \mathbf{Z}^1] - \nabla f(\mathbf{Z}')[\Delta \mathbf{Z}^1] = \int_0^1 \nabla^2 f(\mathbf{Z}(t))[\Delta \mathbf{Z}^1, \mathbf{Z} - \mathbf{Z}'] dt.$$

Taking the supremum over $\|\Delta \mathbf{Z}^1\| \leq 1$ and using the definition of the dual norm,

$$\begin{aligned} \|\nabla f(\mathbf{Z}) - \nabla f(\mathbf{Z}')\|_* &= \sup_{\|\Delta \mathbf{Z}^1\| \leq 1} |\nabla f(\mathbf{Z})[\Delta \mathbf{Z}^1] - \nabla f(\mathbf{Z}')[\Delta \mathbf{Z}^1]| \\ &\leq \int_0^1 \sup_{\|\Delta \mathbf{Z}^1\| \leq 1} |\nabla^2 f(\mathbf{Z}(t))[\Delta \mathbf{Z}^1, \mathbf{Z} - \mathbf{Z}']| dt. \end{aligned}$$

If $\mathbf{Z} = \mathbf{Z}'$, the claim is trivial. Otherwise let $\Delta \mathbf{Z}^2 := \frac{\mathbf{Z} - \mathbf{Z}'}{\|\mathbf{Z} - \mathbf{Z}'\|}$, so that $\|\Delta \mathbf{Z}^2\| = 1$. Then for all $t \in [0, 1]$,

$$\begin{aligned} \sup_{\|\Delta \mathbf{Z}^1\| \leq 1} |\nabla^2 f(\mathbf{Z}(t))[\Delta \mathbf{Z}^1, \mathbf{Z} - \mathbf{Z}']| &= \|\mathbf{Z} - \mathbf{Z}'\| \sup_{\|\Delta \mathbf{Z}^1\| \leq 1} |\nabla^2 f(\mathbf{Z}(t))[\Delta \mathbf{Z}^1, \Delta \mathbf{Z}^2]| \\ &\leq L \|\mathbf{Z} - \mathbf{Z}'\|. \end{aligned}$$

Therefore,

$$\|\nabla f(\mathbf{Z}) - \nabla f(\mathbf{Z}')\|_* \leq \int_0^1 L \|\mathbf{Z} - \mathbf{Z}'\| dt = L \|\mathbf{Z} - \mathbf{Z}'\|.$$

□

Lemma 3. Let $\mathbf{x} \in \mathbb{R}^n$. Then for any $p, q \geq 1$,

$$\|\mathbf{x}\|_{(p, \text{mean})} \leq n^{\max(0, \frac{1}{q} - \frac{1}{p})} \|\mathbf{x}\|_{(q, \text{mean})}.$$

Proof. Proof of Lemma 3. Recall that $\|\mathbf{x}\|_{(p, \text{mean})} = n^{-\frac{1}{p}} \|\mathbf{x}\|_p$. We consider two cases.

Case 1: $p \leq q$. It is well known that $\|\mathbf{x}\|_p \leq n^{\frac{1}{p} - \frac{1}{q}} \|\mathbf{x}\|_q$. Hence,

$$\|\mathbf{x}\|_{(p, \text{mean})} = n^{-\frac{1}{p}} \|\mathbf{x}\|_p \leq n^{-\frac{1}{p}} n^{\frac{1}{p} - \frac{1}{q}} \|\mathbf{x}\|_q = n^{-1/q} \|\mathbf{x}\|_q = \|\mathbf{x}\|_{(q, \text{mean})}.$$

Case 2: $p > q$. In this case, $\|\mathbf{x}\|_p \leq \|\mathbf{x}\|_q$, and therefore

$$\|\mathbf{x}\|_{(p, \text{mean})} = n^{-\frac{1}{p}} \|\mathbf{x}\|_p \leq n^{-\frac{1}{p}} \|\mathbf{x}\|_q = n^{\frac{1}{q} - \frac{1}{p}} \|\mathbf{x}\|_{(q, \text{mean})}.$$

Combining the two cases yields the desired result.

□

Lemma 4. Let $\mathbf{x}, \mathbf{y} \in \mathbb{R}^n$. For any $p, q \geq 1$, we have

$$\|\mathbf{x} \odot \mathbf{y}\|_{(p, \text{mean})} \leq n^{\max(0, \frac{2}{q} - \frac{1}{p})} \|\mathbf{x}\|_{(q, \text{mean})} \|\mathbf{y}\|_{(q, \text{mean})}.$$

Proof. Proof of Lemma 4. By definition,

$$\|\mathbf{x} \odot \mathbf{y}\|_{(p, \text{mean})} = \left(\frac{1}{n} \sum_{i=1}^n |x_i y_i|^p \right)^{1/p}.$$

Applying the Cauchy–Schwarz inequality yields

$$\frac{1}{n} \sum_{i=1}^n |x_i y_i|^p = \frac{1}{n} \sum_{i=1}^n |x_i|^p |y_i|^p \leq \left(\frac{1}{n} \sum_{i=1}^n |x_i|^{2p} \right)^{1/2} \left(\frac{1}{n} \sum_{i=1}^n |y_i|^{2p} \right)^{1/2}.$$

Taking the $1/p$ power on both sides, we obtain

$$\|\mathbf{x} \odot \mathbf{y}\|_{(p, \text{mean})} \leq \|\mathbf{x}\|_{(2p, \text{mean})} \|\mathbf{y}\|_{(2p, \text{mean})}. \quad (14)$$

By Lemma 3 with (p, q) replaced by $(2p, q)$, we have

$$\|\mathbf{x}\|_{(2p, \text{mean})} \leq n^{\max(0, \frac{1}{q} - \frac{1}{2p})} \|\mathbf{x}\|_{(q, \text{mean})}, \quad \text{and} \quad \|\mathbf{y}\|_{(2p, \text{mean})} \leq n^{\max(0, \frac{1}{q} - \frac{1}{2p})} \|\mathbf{y}\|_{(q, \text{mean})}.$$

Combining with (14) gives

$$\|\mathbf{x} \odot \mathbf{y}\|_{(p, \text{mean})} \leq n^{2 \max(0, \frac{1}{q} - \frac{1}{2p})} \|\mathbf{x}\|_{(q, \text{mean})} \|\mathbf{y}\|_{(q, \text{mean})},$$

which proves the claim. □

Lemma 5. Let $\mathbf{x}, \mathbf{y} \in \mathbb{R}^n$. Then for any $p, q \geq 1$,

$$|\langle \mathbf{x}, \mathbf{y} \rangle| \leq n^{\max\{1, \frac{1}{p} + \frac{1}{q}\}} \|\mathbf{x}\|_{(p, \text{mean})} \|\mathbf{y}\|_{(q, \text{mean})}. \quad (15)$$

Proof. Proof of Lemma 5. Let p^* be the conjugate exponent of p , i.e., $\frac{1}{p} + \frac{1}{p^*} = 1$. By Hölder's inequality,

$$|\langle \mathbf{x}, \mathbf{y} \rangle| \leq \|\mathbf{x}\|_p \|\mathbf{y}\|_{p^*}.$$

Moreover, by the definition of (p, mean) norm, i.e., $\|\mathbf{x}\|_p = n^{1/p} \|\mathbf{x}\|_{(p, \text{mean})}$, for any $\mathbf{x} \in \mathbb{R}^n$ and $p \geq 1$, we obtain

$$|\langle \mathbf{x}, \mathbf{y} \rangle| \leq n \|\mathbf{x}\|_{(p, \text{mean})} \|\mathbf{y}\|_{(p^*, \text{mean})}.$$

Thanks to Lemma 3, we have

$$\|\mathbf{y}\|_{(p^*, \text{mean})} \leq n^{\left(\frac{1}{q} - \frac{1}{p^*}\right)_+} \|\mathbf{y}\|_{(q, \text{mean})}.$$

Putting them together yields

$$|\langle \mathbf{x}, \mathbf{y} \rangle| \leq n^{1 + \left(\frac{1}{q} - \frac{1}{p^*}\right)_+} \|\mathbf{x}\|_{(p, \text{mean})} \|\mathbf{y}\|_{(q, \text{mean})}.$$

Finally, since $\frac{1}{p^*} = 1 - \frac{1}{p}$, we have $1 + \left(\frac{1}{q} - \frac{1}{p^*}\right)_+ = \max\left\{1, \frac{1}{p} + \frac{1}{q}\right\}$, which yields the desired result. □